Supporting Information

Sweat pH-enabled strongly adhesive hydrogel for self-powered e-skins

Lei Zhang[a,b], Siheng Wang[a], Zhuomin Wang[a], Zhen Huang[b], Penghao Sun[b], Fuhao Dong[a], He Liu[a], Dan Wang[a]*, Xu Xu[b]**

[a] *Institute of Chemical Industry of Forestry Products, Key Laboratory of Biomass Energy and Material, Jiangsu Province; Key Laboratory of Chemical Engineering of Forest Products, National Forestry and Grassland Administration; National Engineering Research Center of Low-Carbon Processing and Utilization of Forest Biomass; Jiangsu Co-Innovation Center of Efficient Processing and Utilization of Forest Resources, Chinese Academy of Forestry, Nanjing 210042, China.*

[b] *College of Chemical Engineering, Jiangsu Co–Innovation Center of Efficient Processing and Utilization of Forest Resources, Nanjing Forestry University, Nanjing 210037, China.*

* Corresponding authors: liuhe.caf@gmail.com (He Liu); wgdan@163.com (Dan Wang); xuxu200121@njfu.edu.cn (Xu Xu).

Keywords: sweat-pH, hydrogen-bond interactions, tough adhesion, cellulose hydrogel, self-powered e-skin.

Experimental Section

1.1 Materials:

Sodium hydroxide (NaOH, ≥98%), acetic acid (CH_3COOH, ≥99.8%), (2,2,6,6-tetramethylpiperidin-1-yl)oxyl (TEMPO, AR, 99.9%), sodium hypochlorite solution (NaClO, available chlorine content of 13–16%), sodium chlorite ($NaClO_2$, 80%), sodium bromide (NaBr, AR, 99%), acrylic acid (AA, AR, >99%), N,N'-methylenebisacrylamide (MBAA, 99%), and ammonium persulfate (APS, AR, ≥98%) were obtained from Aladdin and used without further purification. Artificial perspirations with different pH values were purchased from Scientific Phygene.

1.2 Fabricating CNFs:

CNFs were prepared by the TEMPO-mediated oxidation of Masson pine wood powder (Shijiazhuang Teng Bang Mineral Products Co. Ltd.).[1] Briefly, NaClO (0.045 mol g^{-1} cellulose) reacted sufficiently to afford TEMPO-oxidized CNFs when the pH of the system was maintained between 10 and 10.2. The prepared CNFs were 9.53 ± 1.7 nm in diameter and 200–800 nm long, as determined from the surface morphology of the nanofibers (Figs. S41 and S42, ESI†). The CNF suspension (approximately 2.1 wt% solid content) was stored at 4 °C for subsequent hydrogel preparation; these CNFs contained 1.76 mmol g^{-1} surface carboxylate groups (Fig. S43, ESI†).[2,3]

1.3 Preparing adhesion hydrogels:

Firstly, acrylic acid (7.2 mL) was slowly added to the abovementioned CNF solution (10 mL) and vigorously stirred until a uniform solution was obtained. The vigorously stirred translucent solution was neutralized by the dropwise addition of aqueous sodium hydroxide (10 g), after which ammonium persulfate (0.125 g) and N,N'-methylenebisacrylamide (0.01 g) were added to the neutralized solution. The uniformly translucent mixture was stirred at room temperature for 0.5 h and then injected into a planar or columnar mold. Hydrogels with various pH values (7.5, 6.5, 5.5, 4.5) were prepared by adjusting the pH of the precursor solution with aqueous NaOH or/and acetic acid, and the pH of each hydrogel was determined using a pH meter (FE28, Mettler Toledo, Switzerland). The CNF/PAA hydrogel was crosslinked by heating at 60 °C for 10 h. A PAA hydrogel was synthesized using the same procedure without the addition of the

CNF solution.

1.4 Characterization:

CLSM (LSM710, Zeiss, Germany) was used to examine the pore structure of each hydrogel when stained with a fluorescent dye. SEM images of the hydrogels prepared at various pH values were acquired using an environmental scanning electron microscope (JSM-7600 Fs, Hitachi, Japan). Variable-pH SAXS data for the various hydrogels were acquired using a SAXSpoint 2.0 apparatus (Anton Paar, Germany). A AVTMR20-010V-I NMR spectrometer (Suzhou Niumag Corporation, China) fitted with a VTMR20-Q-10 mm probe was used measure the relaxation time (T_2) of each hydrogel sample. Raman spectra and spatial Raman maps of the hydrogels were acquired using a Raman imaging microscope (Thermo Scientific DXR2xi, USA) at an excitation laser wavelength of 785 nm. The FTIR spectrum of each hydrogel sample was recorded on a Thermo Fisher spectrometer. The hydrogels were subjected to variable-pH XPS using an AXIS SUPRA+ (Japan) instrument. X-ray diffractometry (XRD) was performed in the 10–60° 2θ range using a D5000 X-ray diffractometer (Siemens, Germany) at 5° min^{-1}. The rheological properties of the hydrogels were examined using a Thermo Fisher Scientific MARS 60 rheometer with a cone-plate geometry (cone angle = 1°, plate diameter = 10 mm). Atomic force microscopy (AFM) was performed using an RTESP-300 (Bruker, USA) instrument. High-resolution solid-state ^{13}C cross-polarization/magic-angle spinning (CP/MAS) NMR spectra of the pulp and CNFs were obtained using a 600 MHz spectrometer equipped with a MAS probe (AVANCE NEO, Bruker, Germany). A pH-adhesive-detachable triboelectric nanogenerator (pAd-TENG) was realized using a linear motor (Linmot E1100). A programmable electrometer (Keithley, model 6514, USA) and a multimeter (Keithley, 7510, USA) were used to determine the open-circuit voltage, short-circuit current, transferred charges, and open voltages during long-term motion cycling.

1.5 Tensile and compressive testing:

Tensile and compression data for the various hydrogel samples with different pH were acquired using a SUNS UTM6503 universal testing machine equipped with a 100-N loading element. Each tensile-tested rectangular hydrogel sample was approximately 20 × 2 mm in size, as measured using calipers. Tensile stress–strain curves were obtained at a continuous stretching rate of 10 mm min^{-1}. A 15-mm-high, 10-mm-diameter cylindrical hydrogel sample was placed

at the center of the lower plate and compressed at a constant loading rate of 5 mm min^{-1} during compression testing. Cyclic tensile and compression testing were performed immediately after initial loading. Three hydrogel samples were examined under each set of conditions and the average results were recorded.

1.6 Adhesion testing:

Interfacial toughness values were determined using 2.5-cm-wide adhered samples using a standard 90-degree peel test (ASTM D2861) with a mechanical testing machine (5-kN load-cell, SANS, UTM6503, China). All data were acquired at a stable peel rate of 50 mm min^{-1}, with test force plateauing when the peeling process approached steady state. Interfacial toughness was determined by dividing the plateau force (obtained by 90-degree peel testing) by the width of the sample.

A sample with a 2.5 × 1 cm adhered area was subjected to standard lap shear testing (ASTM F2255) using the abovementioned mechanical testing machine. All data were acquired at a steady peel rate of 50 mm min^{-1}. Shear strength was calculated by dividing maximum force by bond area.

A sample with a 2.5 × 2.5 cm adhered area was subjected to standard tensile testing (ASTM F2258) using the abovementioned mechanical testing machine. All data were acquired at a steady peel rate of 50 mm min^{-1}. Tensile strength was calculated by dividing maximum applied force by adhesion area.

1.7 CNF/PAA hydrogels biocompatibility:

Prepared extracts were placed in the wells of standard 96-well cell culture plates in a certified A2 biosafety cabinet, and seeded with 500,000 L929 mouse fibroblasts per well after ethanol/UV sterilization. Cells were further treated with trypsin-EDTA (Gibco) and resuspended in extracts. Cells were seeded at a density of 1×10^3 into each well of the 96-well plate and allowed to grow for 48 h. Hydrogel cytocompatibility of the was analyzed using a Cell Counting Kit 8 (CCK-8) assay (Bimake), and a live/dead assay, and 2 μM Calcein AM (in DPBS) and 4 μM EthD-1 (Invitrogen) working solution. The 96-well plate was incubated at 37 °C for 20 min in a 5% CO_2 incubator. Cell morphologies were observed by fluorescence microscopy. Six parallel experiments were conducted for each group to obtain convincing results.

1.8 Ionic conductivity:

The electrochemical impedance spectrum of each hydrogel was acquired using an electrochemical workstation (CORRTEST, CS310H, China) in the 10^{-1} to 10^{-5} Hz frequency range at a voltage of 100 mV. The ionic conductivities of the various hydrogels were calculated using the equation:

$$\sigma = \frac{L}{RA}$$

where L is the distance between the two probes, R is the electrical resistance entire hydrogel, and A is the cross-sectional area of the hydrogel.

1.9 Preparing the pH-adhesive-detachable triboelectric nanogenerator (pAd-TENG):

The pAd-TENG consisted of a CNF/PAA hydrogel substrate and a silicone rubber layer (polydimethylsiloxane, PDMS) as the tribonegative material. Before heat curing, the CNF/PAA precursor was injected into a rectangular groove mold fitted with a 340-mm Pi tape spacer. The signal readout wires were immersed in the hydrogel solution to facilitate connecting the hydrogel electrodes to external circuits, which bonded within the hydrogel as it solidified. The PDMS elastomer layer was further fabricated by blade-coating a well-mixed mixture of commercially available silicone (1:10 w/w Sylgard184 parts A and B) on the prepared hydrogel layer, after which it was cured at 80 °C for 2 h. All devices used in this study were 3 × 3 × 2 cm in size.

1.10 Demonstrating real-life applications:

Experiments were performed with the assistance of volunteers, and informed consent was obtained for image and data release. Assembled sensors were attached to various parts of the human body, including the fingers, elbows, feet, and knees, and voltage changes resulting from various actions or long-term movements were recorded in real time using digital electrometers.

Supplementary Figures:

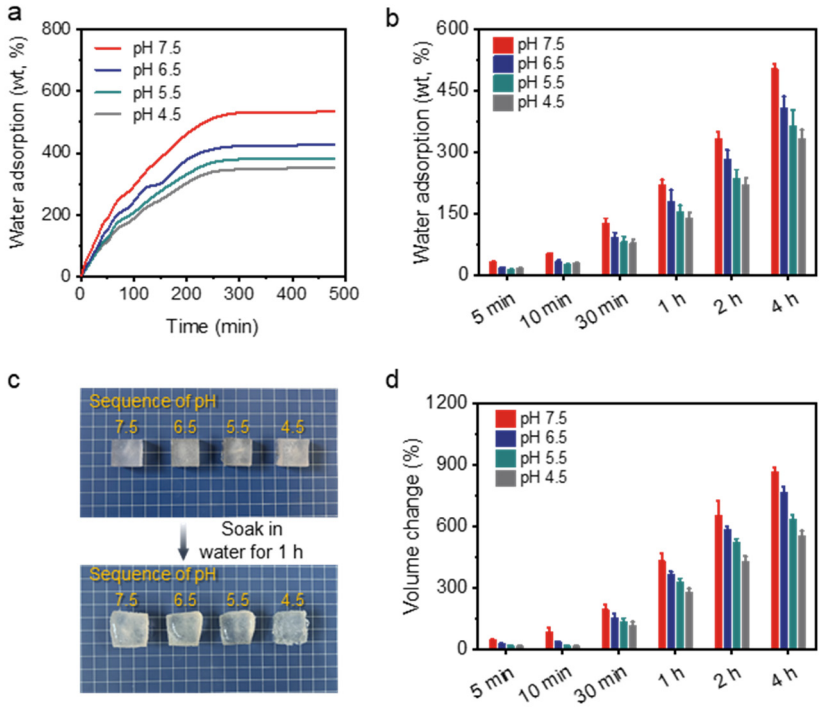

Fig. S1. (a) Water absorption curves and (b) comparisons of CNF/PAA hydrogels with different pH accompanied by swelling time. (c) Photographs of CNF/PAA hydrogels with different pH before and after soaking in water for 1 h. (d) Comparisons of volume change of CNF/PAA hydrogels with different pH accompanied by swelling time.

As shown in Fig. S1a, with the prolongation of immersion time, the water absorption of CNF/PAA hydrogels display an upward trend at varying pH and reach equilibrium swelling within 4 h. However, an interesting swelling behavour is found that the equilibrium swelling at relatively low pH is lower than that at relatively high pH. In particular, the equilibrium water absorption of the hydrogel at pH 7.5 and 4.5 is 504.1% and 334.3%, respectively, which is attributed to the protonation of PAA at relatively low pH conditions (Fig. S1b). Furthermore, we further explored the volume swelling of hydrogels at different pH, and we found that even after soaking in water for 1 h, all the hydrogels presented only slight swelling, indicating a considerable swelling property (Fig. S1c). While the volume change trend of hydrogels is similar to that of water absorption, revealing a protonated inducer at relatively low pH (Fig. S1d).

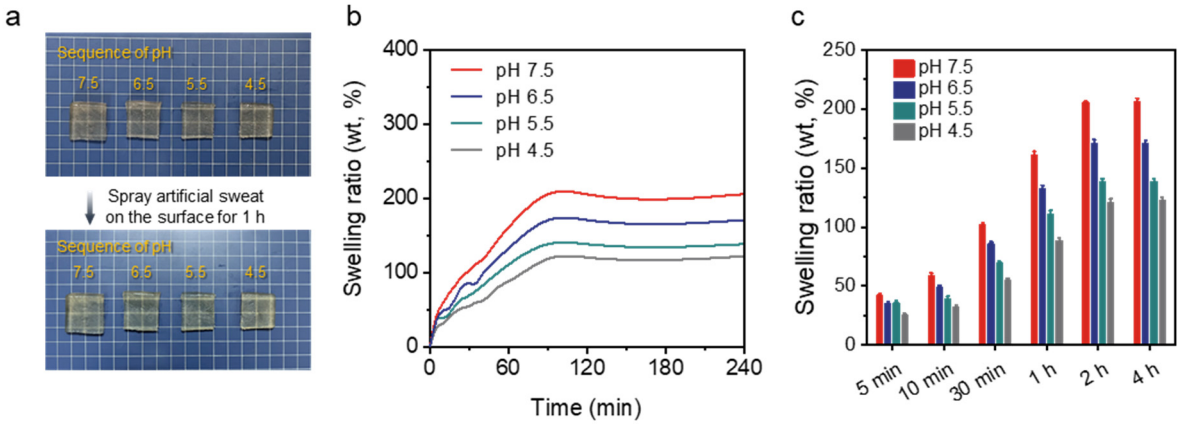

Fig. S2. (a) Photographs of before and after spraying artificial sweat with different pH on the surface of the CNF/PAA hydrogel for 1 h, and replenishing the artificial sweat every 10 min. (b) Swelling ratio curves and (c) comparisons of CNF/PAA hydrogels soaked in artificial sweat with different pH along with swelling time.

We further explored swelling properties of the CNF/PAA hydrogel in artificial sweat with different pH. As shown in Fig. S2a, thorugh spraying artificial sweat with different pH on the surface of the CNF/PAA hydrogel with pH 7.5 for 1 h, taking 10 min as a cycle of replenishing artificial sweat. It can be observed that all hydrogel exhibit negligible volume expansion in the whole range of the artificial sweat pH, indicating an excellent stability in sweat pH. Furthermore, we quantitatively analyzed swelling rates of the hydrogel in artificial sweat with different pH. As shown in Fig. S2b, with the increase of the soaking time, hydrogels present an increasing swelling rate, while the swelling equilibrium is basically reached when soaking the hydrogel for 2h. Notably, with decreasing pH, the hydrogel exhibits a lower equilibrium swelling rate, implying a better stability. Specifically, when the swelling equilibrium is completely reached (soaking for 4 h), swelling ratios of the hydrogel in artificial sweat at pH 7.5, 6.5, 5.5 and 4.5 are 206.1%, 171.3%, 138.9% and 122.4%, respectively (Fig. S2c). Although an echelon decrease in the equilibrium swelling rate can be found with the decrease of pH, the ultimate difference in swelling rate is only 83.7% without intolerable gap, indicating that the hydrogels are still capable to resist severe swelling in sweat with various pH, which is attributed to a stable hydrogen bond network structure of the hydrogel.

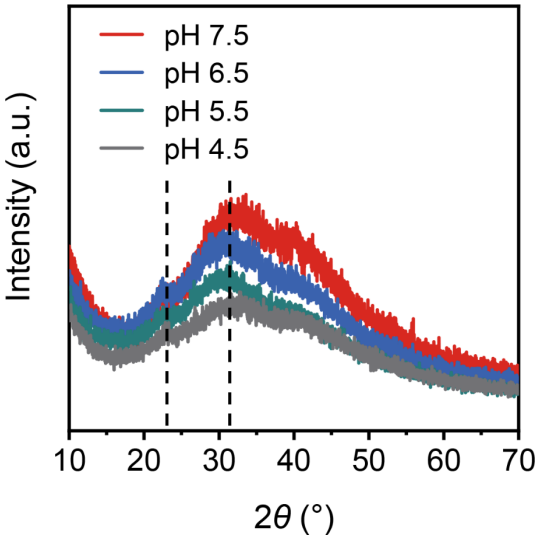

Fig. S3. X-Ray diffraction (XRD) spectroscopy of the CNF/PAA hydrogel in the different pH.

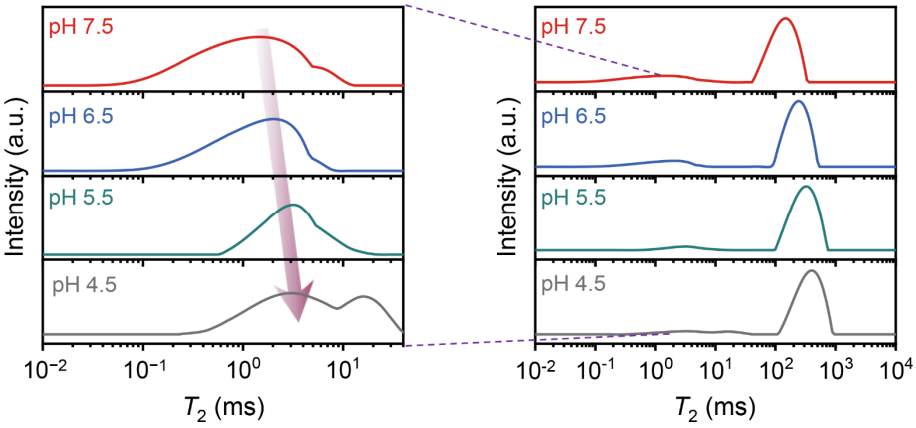

Fig. S4. Low-field (LF) NMR spectra of the CNF/PAA hydrogel as the pH decreased.

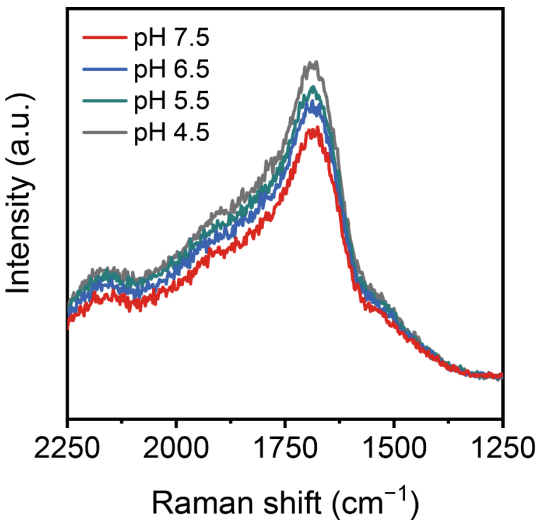

Fig. S5. Raman spectra of the CNF/PAA hydrogel during the pH decreasing process.

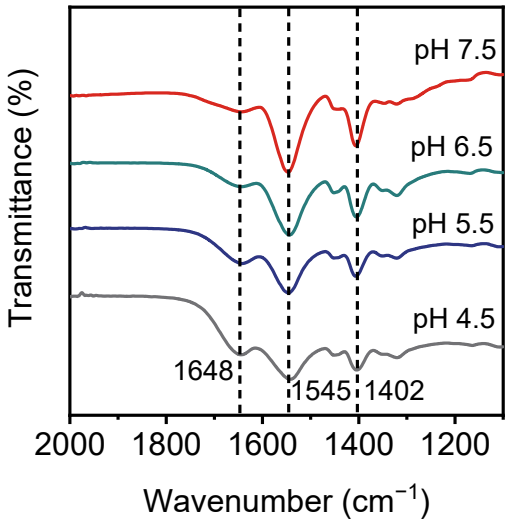

Fig. S6. Fourier-transform infrared (FTIR) investigations on various dry CNF/PAA hydrogels in different pH.

for the CNF/PAA hydrogel at pH 7.5 sample, three main characteristic peaks related to the carboxyl group are found, among which the peak at 1648 cm^{-1} belongs to the C=O stretching of the protonated carboxyl group (as the −COO^{-}), The vibrational peaks at 1545 and 1402 cm^{-1} correspond to the asymmetric and symmetric stretching of the deprotonated carboxyl group (as the −COOH), respectively, indicating an existence of both protonated and deprotonated acidic functional groups under this condition. As the pH decreases within the hydrogel system, the enhancement of protonated characteristic peak for −COOH, and the diminishing of deprotonated characteristic peaks for −COO^{-} can be observed, suggesting that the carboxyl group gradually shifts from the deprotonated to the protonated state with the drop of pH. Therefore, we can conclude that the accompanying pH drop from 7.5 to 4.5 in the CNF/PAA hydrogel system tends to enable the conversion of deprotonated states for −COO^{-} to protonated states for −COOH.

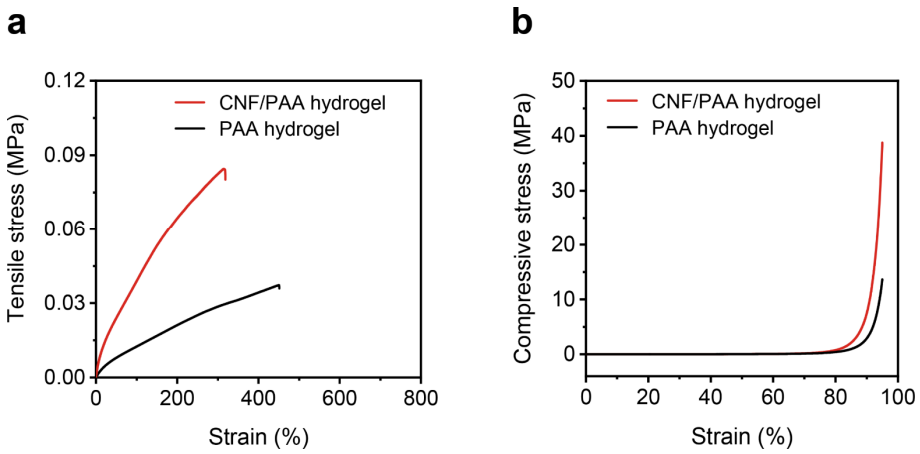

Fig. S7. Mechanical properties of the CNF/PAA, PAA hydrogels. (a) Tensile strain-stress curves of the CNF/PAA, PAA hydrogels. (b) Compressive strain-stress curves of the CNF/PAA, PAA hydrogels.

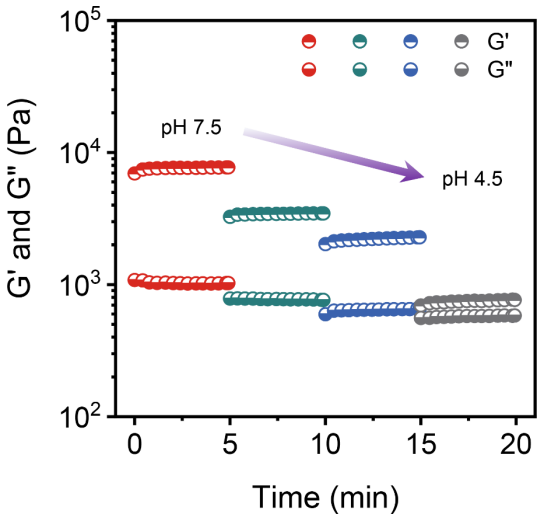

Fig. S8. Rheological behavior of the CNF/PAA hydrogel in a continuous process of switchable pH.

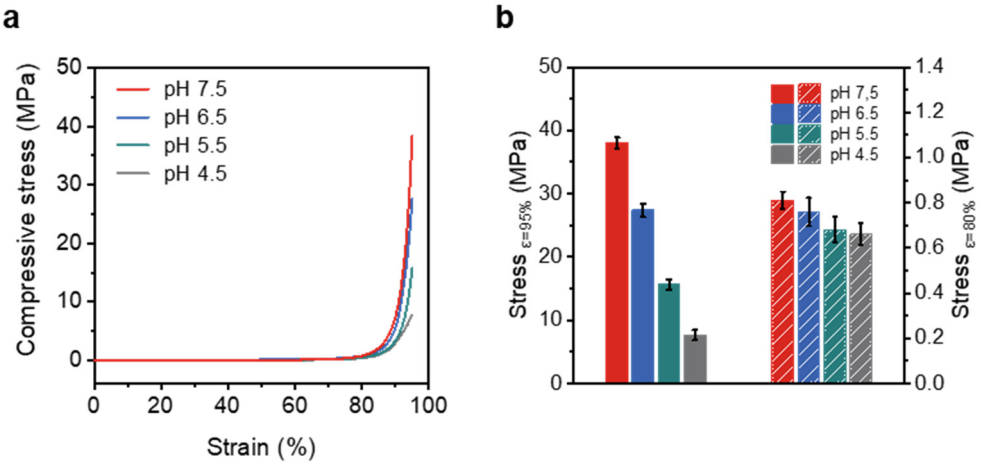

Fig. S9. Comparsion of the mechanical performance of the CNF/PAA hydrogel with other adhesive materials.

As shown in Fig. S9a, the compressive stress of the CNF/PAA hydrogels shows a decaying trend with the decrease of pH, and the ultimate compressive strain of all the hydrogels reaches 95%, displaying a supercompressibility. Typically, a compressive strength ($stress_{\varepsilon=95\%}$) of 38.39 MPa is observed at pH 7.5, whereas this is only 7.69 MPa at pH 4.7, which corresponds to a 79.9% decrease due to the destruction of the H-bonded network by excess hydronium ions. As expected, a similar mechanical behavior is exhibited for the compressive stress at a strain of 80%, that is, the corresponding $stress_{\varepsilon=80\%}$ decreases from 0.81 MPa to 0.66 MPa, accompanied by a drop in pH from 7.5 to 4.5 (Fig. S9b).

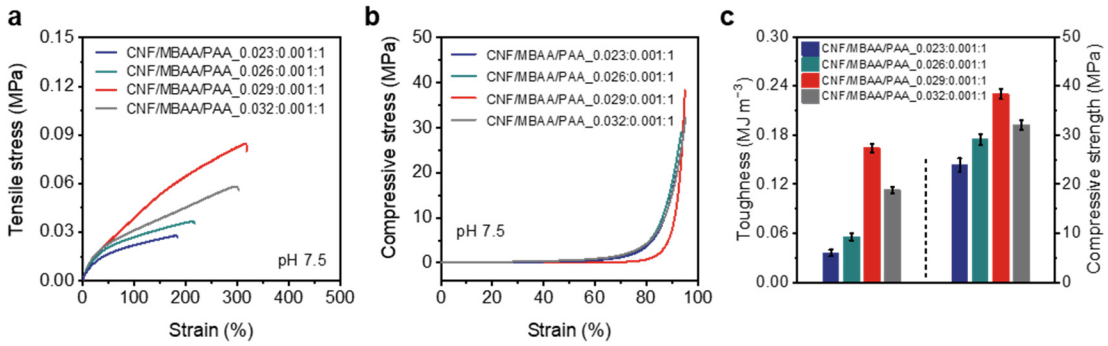

Fig. S10. (a) Tensile and (b) compressive stress-strain curves of CNF/PAA hydrogels prepared with different material ratios at pH 7.5. (c) Comparison of toughness and compressive strength of CNF/PAA hydrogels prepared with different material ratios at pH 7.5.

The tensile stress-strain curves of various hydrogels at pH 7.5 are shown in Fig. S9a. It can be observed that when the mass ratio of CNF to PAA is less than 0.029: 1, both the ultimate tensile stress and fracture strain of the CNF/PAA hydrogel display an increasing trend with the increase of CNF content, which is attributed to the introduction of CNF to enhance the combination with PAA and promote a stronger hydrogen bond network structure. However, continuing to add CNF to the system would lead to an inhomogeneous mixture, resulting in a decrease in the tensile properties of the hydrogel. In particular, when the mass ratio of CNF vs. MBAA vs. PAA is 0.029: 0.001: 1, the hydrogel exhibits the best tensile properties, that is, the ultimate tensile stress is 0.084 MPa corresponding to a fracture strain of 315%.

For compression tests, a similar mechanical behavior is observed, that is, when the mass ratio of CNF to PAA is less than 0.029: 1, the fracture compressive stress of the hydrogel presents an upward trend with increasing CNF due to the enhanced hydrogen bond network; and when the mass ratio of CNF to PAA is higher than 0.029: 1, the increased CNF actually lead to the opposite because of the non-uniform system (Fig. S10b). Typically, the hydrogel shows the highest toughness of 0.16 MJ m^{-3} and compressive strength of 38.39 MPa when the mass ratio of CNF vs. MBAA vs. PAA is 0.029: 0.001: 1 (Fig. S10c).

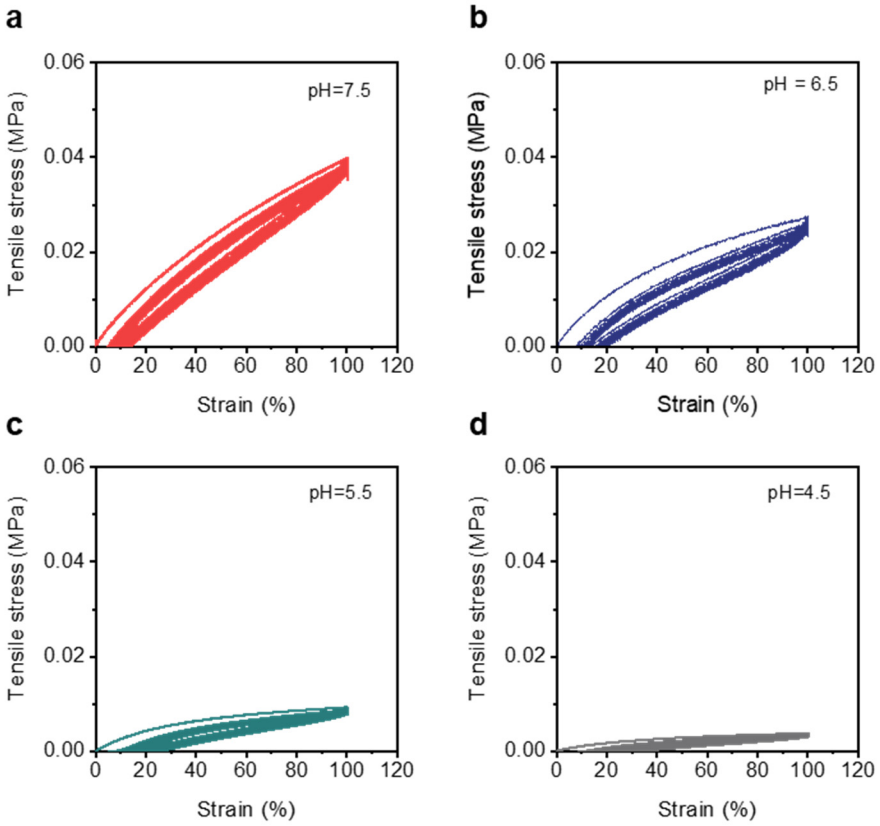

Fig. S11. Cyclic mechanical properties of the CNF/PAA hydrogel in the different pH. (a−d) Cyclic tensile strain-stress curves of the CNF/PAA hydrogel in the different pH (7.5, 6.5, 5.5, 4.5).

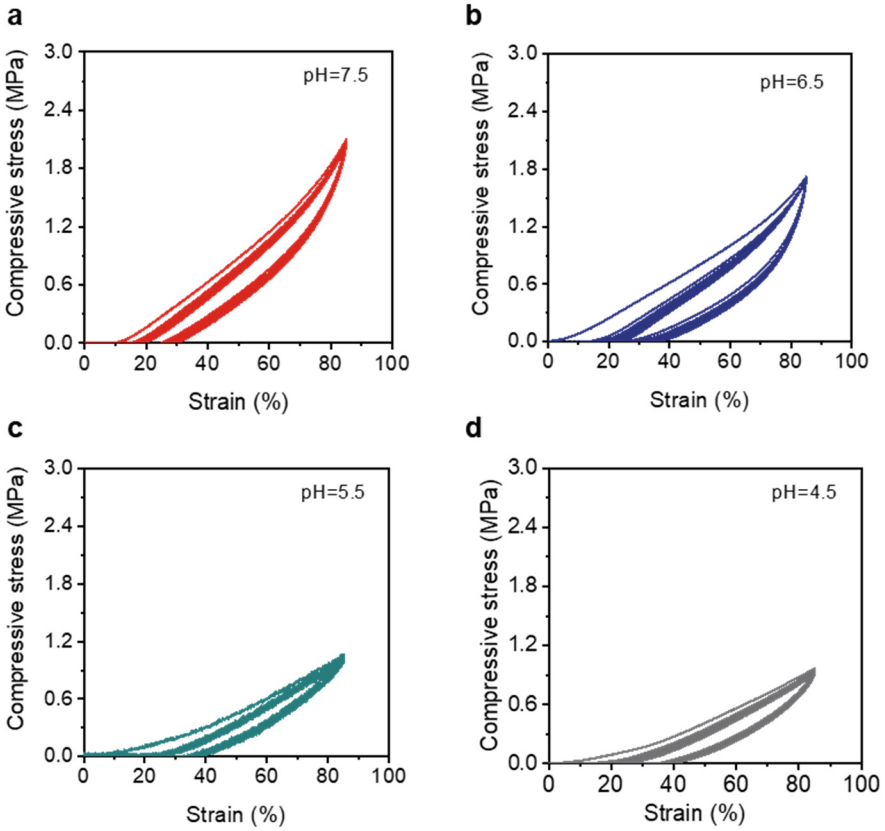

Fig. S12. Cyclic mechanical properties of the CNF/PAA hydrogel in the different pH. (a−d) Cyclic compressive strain-stress curves of the CNF/PAA hydrogel in the different pH (7.5, 6.5, 5.5, 4.5).

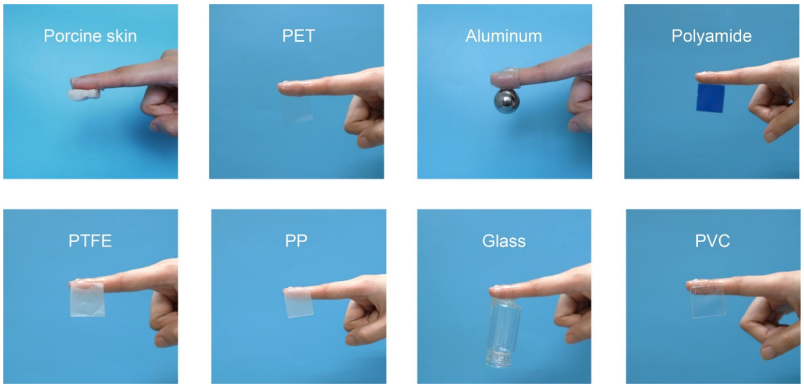

Fig. S13. Photographs of the CNF/PAA hydrogel with excellent adhesion to various representative substrates. The CNF/PAA hydrogel could be firmly adhered to human fingers and different substrates without obvious peeling gaps, which indicated that the as-prepared hydrogel had excellent and Wide range of adhesion properties.

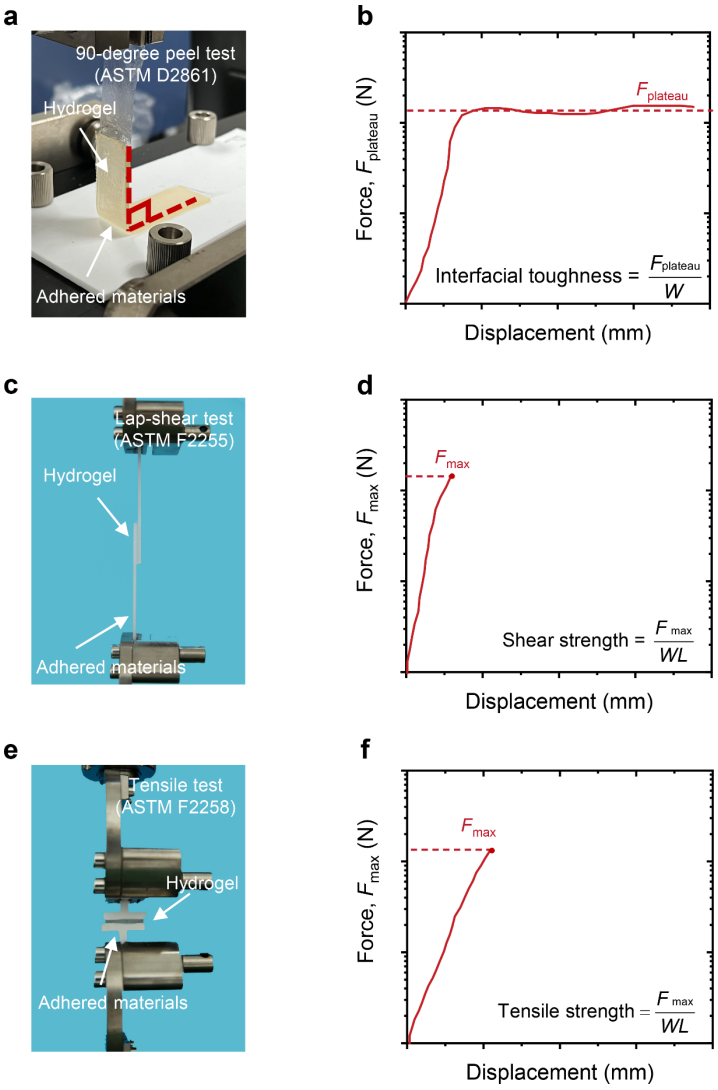

Fig. S14. Setups for mechanical testing of adhesion performance of the CNF/PAA hydrogel. (a, b) Photograph and setup for measurement of interfacial toughness based on the standard 90-degree peel test (ASTM D2861). (c, d) Photograph and setup for measurement of shear strength based on the standard lap-shear test (ASTM F2255). (e, f) Photograph and setup for measurement of tensile strength based on the standard tensile test (ASTM F2258). F force; $F_{plateau}$, plateau force in a peeling test; F_{max}, maximum force in the lap-shear and tensile test; L, length; W, width.

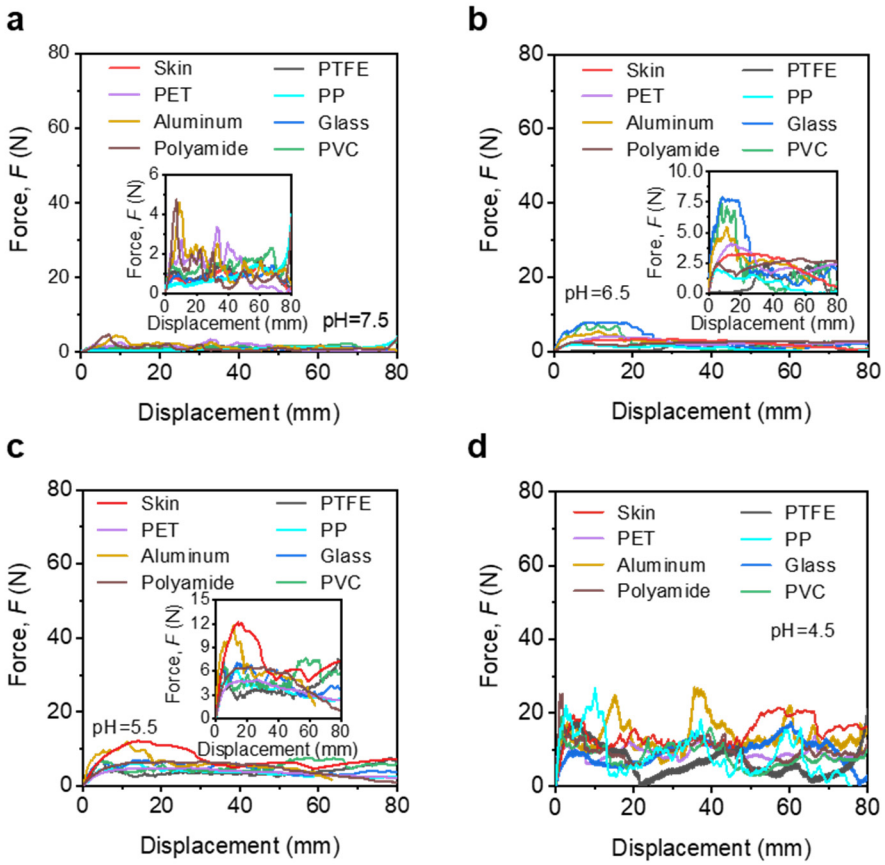

Fig. S15. Comparison of peel test plateau force of the CNF/PAA hydrogel to different substrates in the different pH. (a−d) 90-degree peel test curve of the CNF/PAA hydrogel in the different pH.

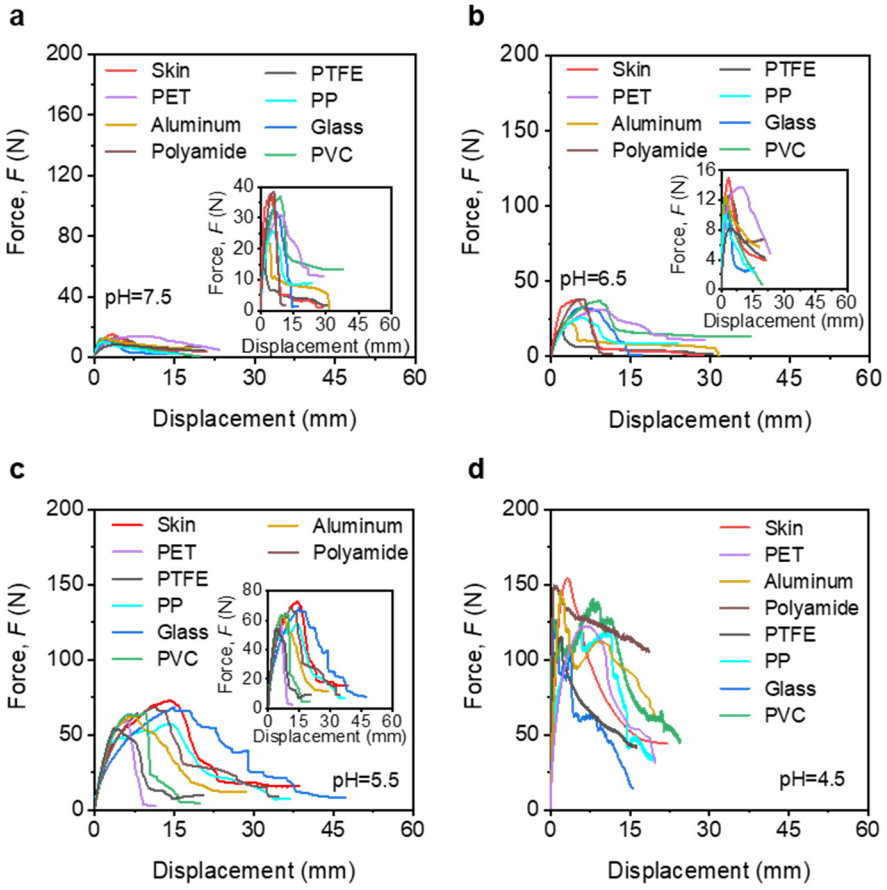

Fig. S16. Comparison of lap-shear test max force of the CNF/PAA hydrogel to different substrates in the different pH. (a−d) Lap-shear test curve of the CNF/PAA hydrogel in the different pH.

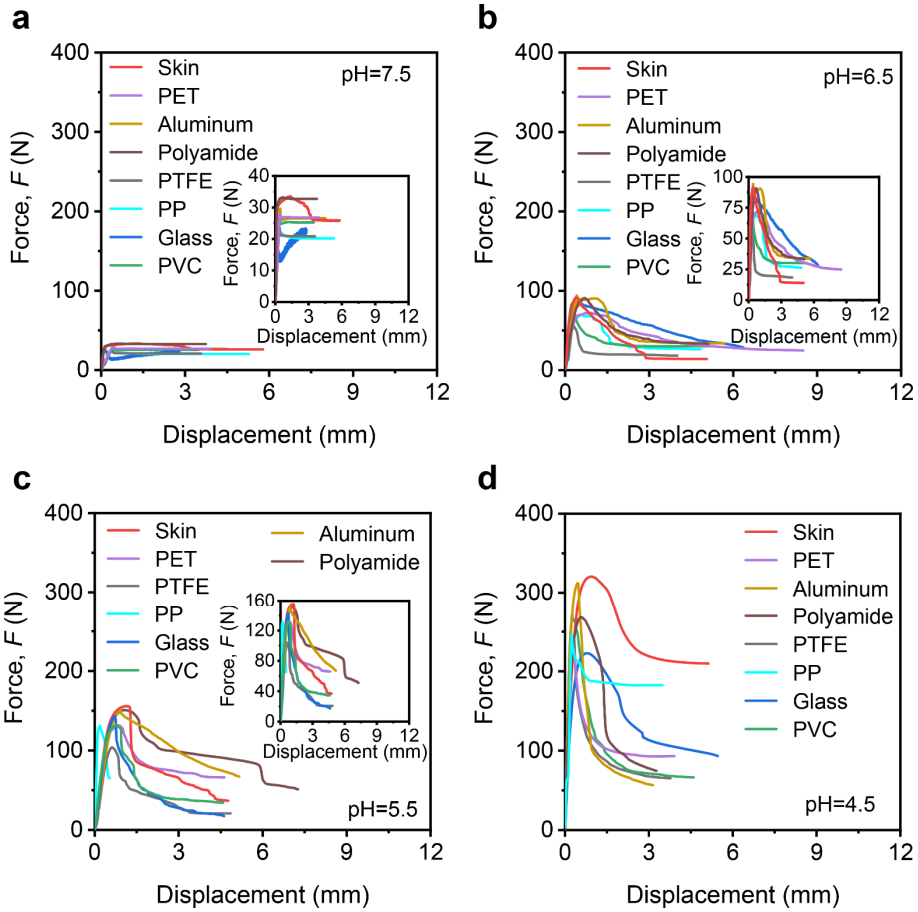

Fig. S17. Comparison of tensile test max force of the CNF/PAA hydrogel to different substrates in the different pH. (a–d) Tensile test curve of the CNF/PAA hydrogel in the different pH.

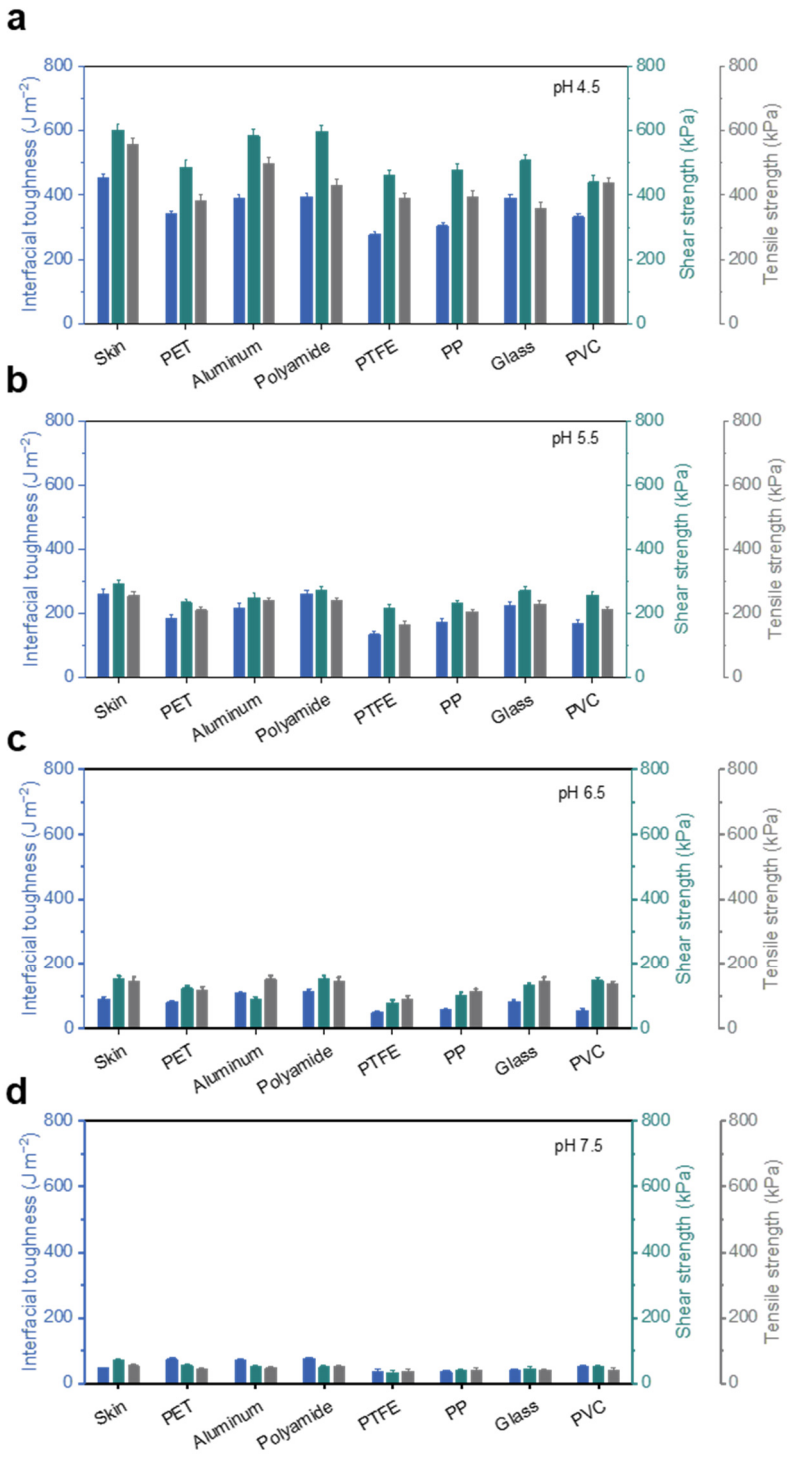

Fig. S18. Comparison of adhesion strength of the CNF/PAA hydrogel detached from different substrates under four conditions, including pH 4.5, pH 5.5, pH 6.5, pH 7.5, respectively. (a−d) Comparison of interfacial toughness, shear strength, and tensile strength of the CNF/PAA hydrogel detached from different substrates under four conditions respectively (including pH 4.5, pH 5.5, pH 6.5, pH 7.5).

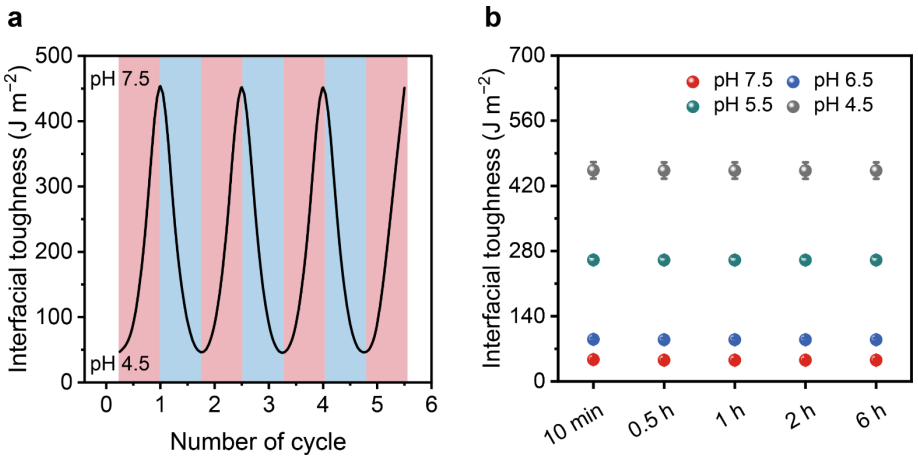

Fig. S19. Interfacial toughness as a function of several variables. (a) Cyclic interfacial toughness of the CNF/PAA hydrogel as the pH changed continuously. (b) Interfacial toughness of the CNF/PAA hydrogel maintains stable as the adhesion time increased. The experiment for each value of the variable was repeated with three samples.

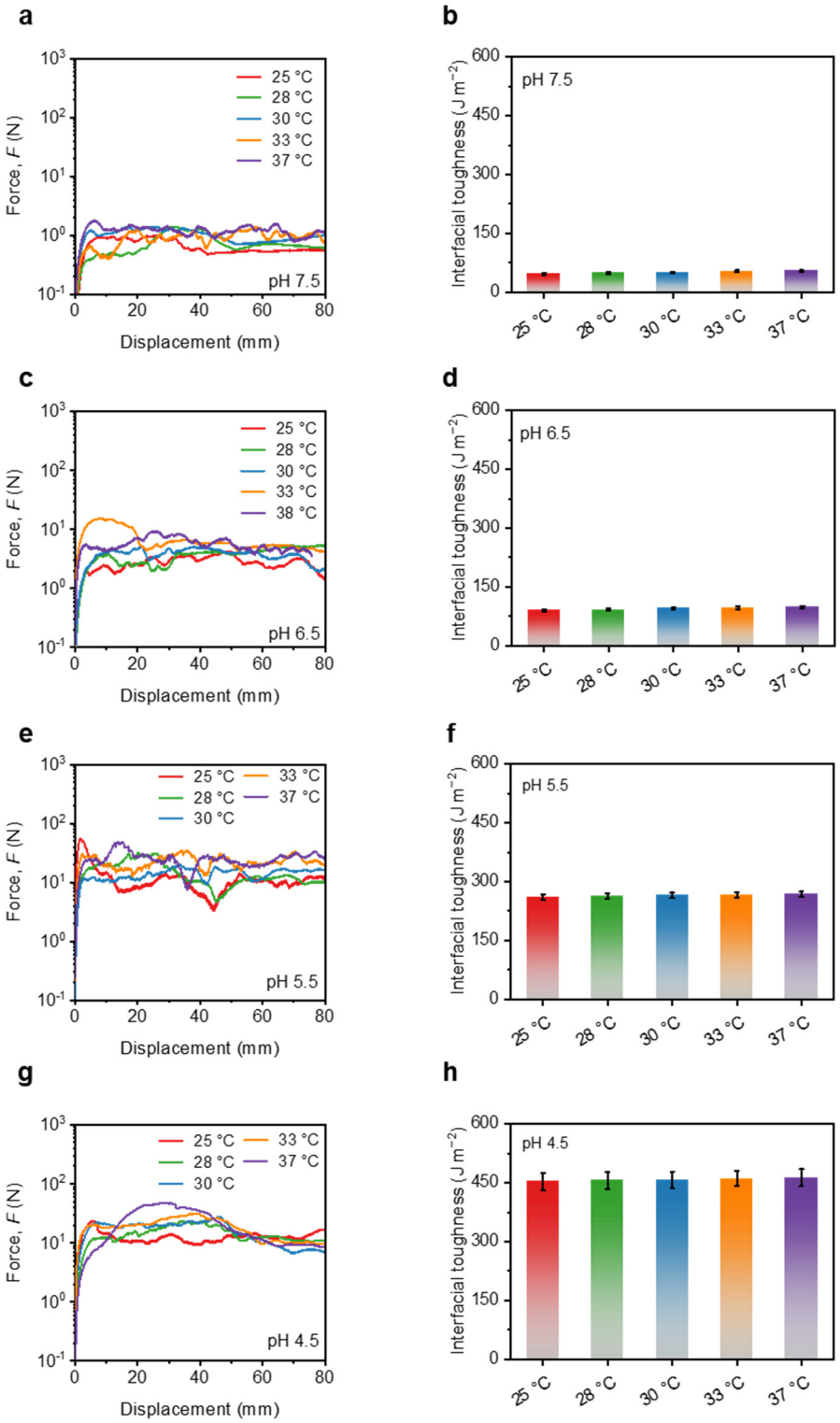

Fig. S20. Plateau force–displacement curves for the CNF/PAA hydrogel on skin at pH 7.5 (a), 6.5 (c), 5.5 (e), and 4.5 (g), respectively. Interfacial toughness for the CNF/PAA hydrogel on skin at pH 7.5 (b), 6.5 (d), 5.5 (f), and 4.5 (h), respectively.

For any CNF/PAA hydrogel at the same pH, it can be observed that the peeling platform force does not change significantly even at elevated temperatures, which indicates that the

CNF/PAA hydrogel is capable to be insensitive to temperature in adhesion. In particular, the interfacial toughness of the PAA/CNF hydrogel at pH 4.5 reaches 453.47 and 462.68 J m^{-2} at 25 and 37 °C respectively, showing negligible differences, which demonstrates a stable adhesive hydrogel over a wide epidermal skin temperature range. Notably, although exhibiting similar adhesive behavior of CNF/PAA hydrogels at pH 7.5, their interfacial toughness is approximately 50 J m^{-2} at varied temperatures, indicating that it maintains high adhesion to the skin. Additionally, for CNF/PAA hydrogels at uniform temperature (such as 25 °C), the interfacial toughness increases sharply with the decrease of pH, revealing that pH is the most important factor for enhancing the adhesion performance of the hydrogel compared to the negligible temperature dependence.

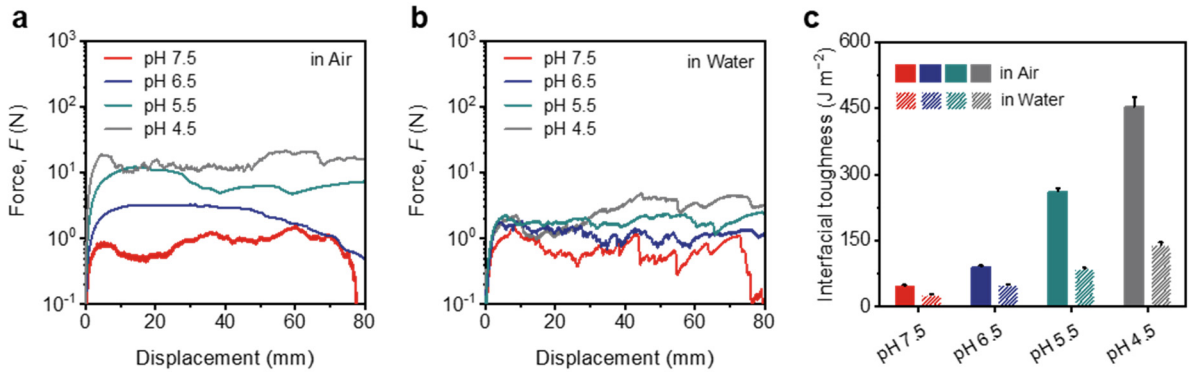

Fig. S21. The force-displacement curves of CNF/PAA hydrogels with different pH in (a) air and (b) water obtained by 90-degree peel test on skin. (c) Comparison of interfacial toughness of CNF/PAA hydrogels with different pH in air and water on skin.

The 90-degree peel force curves of CNF/PAA hydrogels with different pH in air and water are shown in Fig. S21a and S21b, respectively. For the peel tests both in air and water, a rising peel force is exhibited with decreasing pH, which is associated about the excess hydronium ions disrupting the hydrogen bond network structure resulting in more active groups and thus improving adhesion. Although, a significant decrease in the platform peel force is found in water compared to that in air, the platform peel force is still higher than 1 N, indicating a good adhesion. Furthermore, the interfacial toughness is obtained, where the interfacial toughness of the CNF/PAA hydrogel at pH 4.5 in air and water are 453.47 and 138.64 J m^{-2}, respectively, showing an inevitable decrease in water but still above 100 J m^{-2}, and remaining an expectant advantage (Fig. S21c).

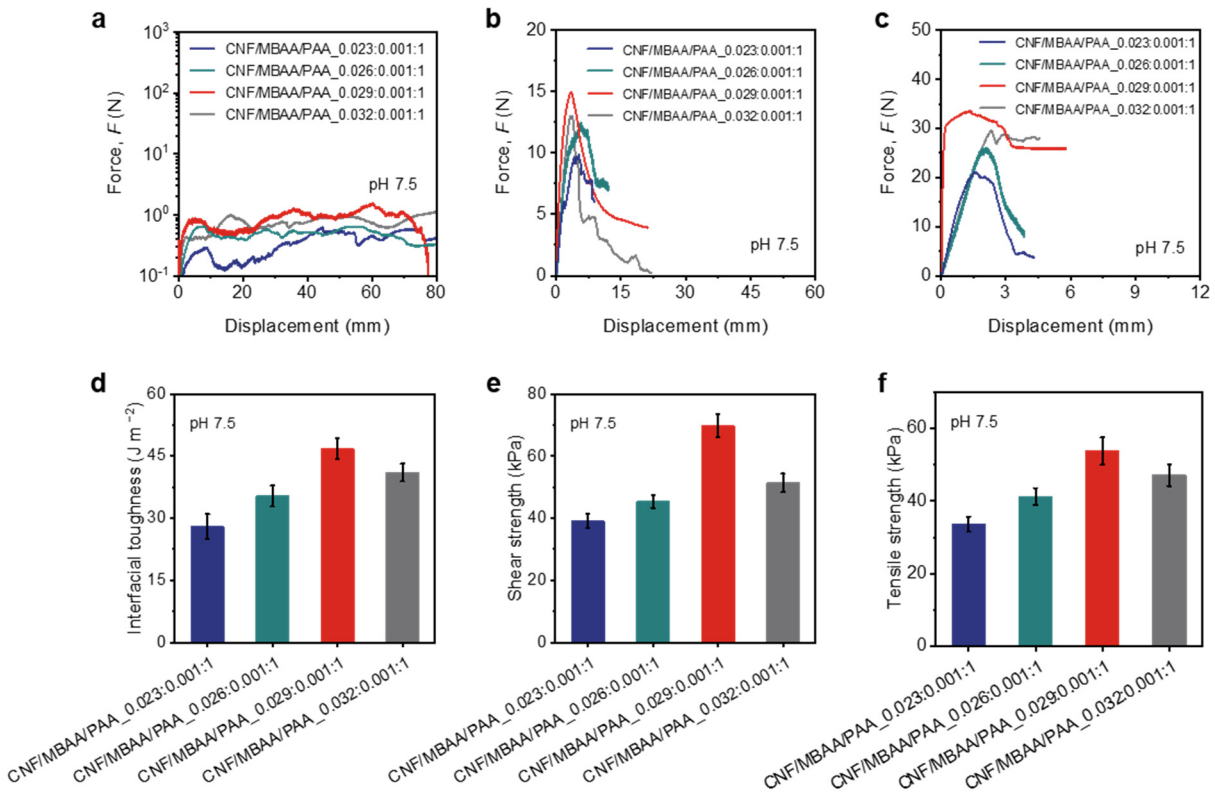

Fig. S22. The force-displacement curves of CNF/PAA hydrogels with different material ratios obtained by 90-degree peel (a), lap-shear (b), and tensile (c) tests on skin at pH 7.5, respectively. Comparison of interfacial toughness (d), shear strength (e), and tensile strength (f) of CNF/PAA hydrogels prepared with different material ratios at pH 7.5.

In order to explore the adhesive properties of CNF/PAA hydrogels at pH 7.5 prepared with different material ratios, we performed 180-degree peeling, lap-shear and tensile tests on freshly excised porcine skin, and the obtained force-displacement curves were shown in Fig. S22a, S22b and S22c, respectively. According to these force-displacement curves, we can find that, when the mass ratio of added CNF to PAA is less than 0.029: 1, as the CNF increases, the peel force, shear force, and tensile force all show an rised trend, which becauses that the introduction of CNF has a positive effect on the cohesive energy of the hydrogel, prompting more active groups to bond with groups on the skin surface. As expected, the peeling force, shear force and tensile force of hydrogels show an attenuation when CNF is continued to be added, which is asscribed to the excess CNF resulting in a non-uniform hydrogel, enabling it easily friable to a weak adhesion on the skin.

More intuitively, the interfacial toughness (Fig. S22d), shear strength (Fig. S22e), and

tensile strength (Fig. S22f) of CNF/PAA hydrogels at pH 7.5 on skin were correspondingly obtained, respectively, and a similar adhesion trend to that of the force-displacement curves could be found. Specifically, when the mass ratio of CNF vs. MBAA vs. PAA is 0.029: 0.001: 1, the hydrogel exhibits a 46.74 J m^{-2} for interfacial toughness, a 69.71 kPa for shear strength, and a 53.67 kPa for tensile strength at pH 7.5. These impressive adhesion observations reveal a CNF/PAA hydrogel with excellent adhesion properties through an optimal material ratio, that is, a mass ratio of CNF vs. MBAA vs. PAA is 0.029: 0.001: 1.

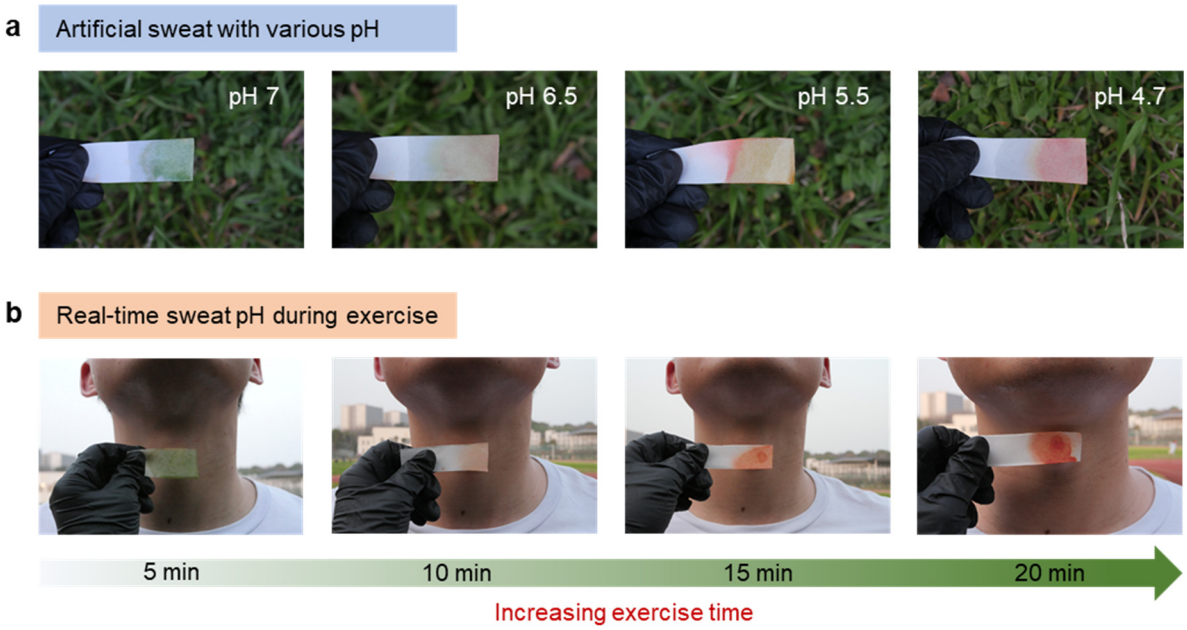

Fig. S23. (a) Photographs of test strips with artificial sweat of different pH under the action of pH indicator. (b) Photographs of test strips with sweat pH of volunteer during exercise under the action of a pH indicator.

As showed in Fig. S23a, it can be observed that the colour change of test strips with artificial sweat is blue-green to yellow-blue to yellow-orange with the change of pH from 7 to 6.5 to 5.5 to 4.7 under the action of the pH indicator, which is in good agreement with the results of the recently reported work[3, 4]. Furthermore, we measured the real-time sweat pH of the volunteers during running (Fig. S23b). We found that with a increasing exercise time, the colour change trend of test strips with the sweat of the volunteers was similar to that of the corresponding artificial sweat, indicating a droped pH states during exercise due to the release of hydronium ions when sweating.

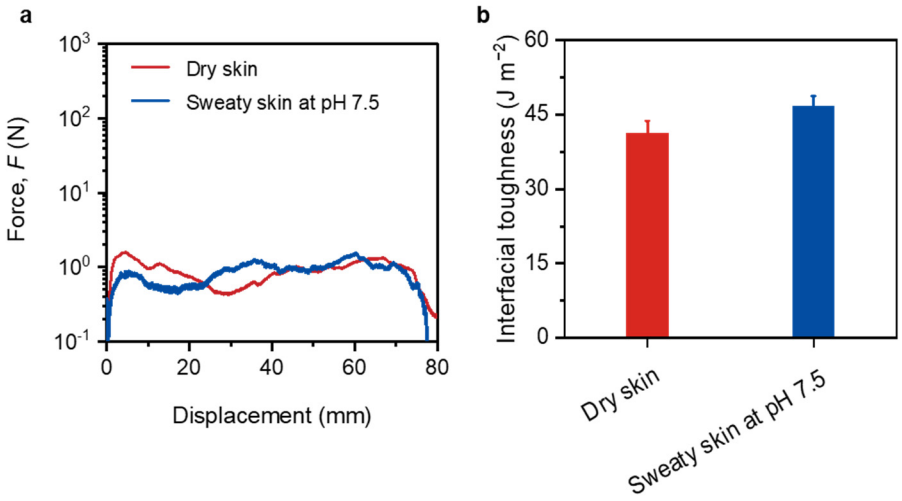

Fig. S24. (a) Plateau force–displacement curves and (b) interfacial toughness for the CNF/PAA hydrogel when applied to the dry skin and sweaty skin at pH 7.5.

As shown in Fig. S24a, the CNF/PAA hydrogel exhibits similar peel force-displacement curves on dry skin and sweaty skin at pH 7.5, indicating that the hydrogel has similar adhesion properties on both dry and sweaty skin. Specially, the interfacial toughness of the hydrogel is 41.30 J m^{-2} on dry skin and 46.74 J m^{-2} on sweaty skin at pH 7.5, displaying a slight difference, which demonstrates a good adhesion performance when the hydrogel applied on dry skin (Fig. S24b). Therefore, the CNF/PAA hydrogel adheres to the skin and is completely conformable to a variety of physiological conditions including dry and sweaty state.

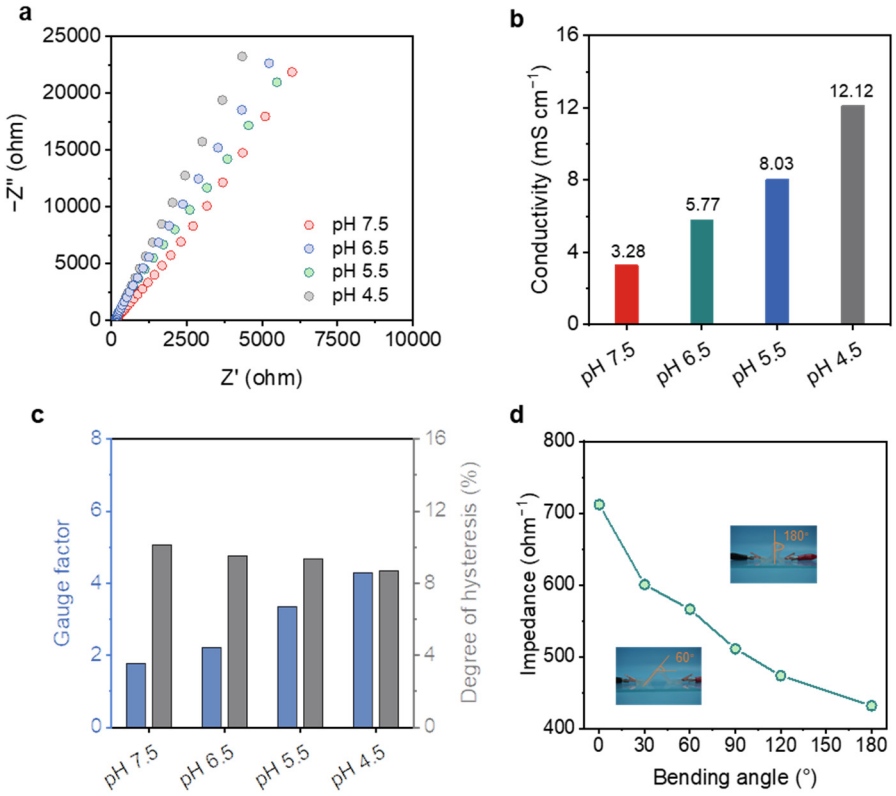

Fig. S25. (a) EIS Nyquist plot of the CNF/PAA hydrogel in the different pH. (b) Ionic conductivity of the CNF/PAA hydrogel in the different pH. (c) Comparison of gauge factor and degree of hysteresis of the CNF/PAA hydrogel in the different pH. (d) Impedance of the CNF/PAA hydrogel at pH 4.5 for different bending angles.

To evaluate conductive performance of CNF/PAA hydrogels at different pH, we performed electrochemical AC impedance measurements by incorporating hydrogels into equivalent circuits. As shown in Fig. S25a, the Nyquist plots of CNF/PAA hydrogels at different pH were obtained, where the intercept of the scatter plot with the x-axis represents the internal resistance of the hydrogels according to literature reports[1]. It can be found that as the pH decreases, the hydrogel exhibits a decreasing internal resistance, indicating that it has better ionic conductivity. Furthermore, we calculated the ionic conductivity of CNF/PAA hydrogels at different pH, and as expected, CNF/PAA hydrogels exhibit increased the ionic conductivity with decreasing pH from 7.5 to 4.5; typically, corresponding to 3.28 mS cm^{-1} at pH 7.5, and 12.12 mS cm^{-1} at pH 4.5, an increase of 2.70 times, showing excellent ionic conductivity with low pH dependence (Fig. S25b).

Furthermore, we explored the sensing performance of CNF/PAA hydrogels with different

pH, as shown in Fig. S25c, with the decrease of pH, the hydrogels showed an increasing gauge factor, which is consistent with the results of ionic conductivity. Among them, the gauge factor of CNF/PAA hydrogel reached 1.76 and 4.28 at pH 7.5 and pH 4.5, respectively, and the reduced pH promoted a 1.43-fold increase in the gauge factor; meanwhile, a low hysteresis was accompanied, which together reveals impressive sensing performance in the whole sweat pH range. In addition, we conducted the impedance change of the CNF/PAA hydrogel at pH 4.5 and bent it at varying angles, as well as found that the impedance changed responsively with various bending angle, further implying its excellent sensing performance (Fig. S25d).

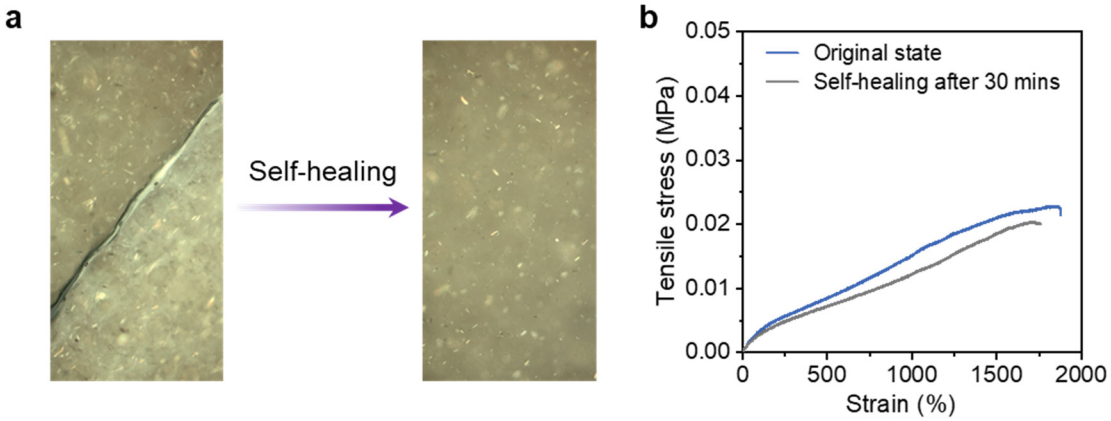

Fig. S26. Self-healing properties of the CNF/PAA hydrogel. (a) Photographs of the self-healing properties of the CNF/PAA hydrogel. (b) Tensile stress-strain curves of the self-healing hydrogel.

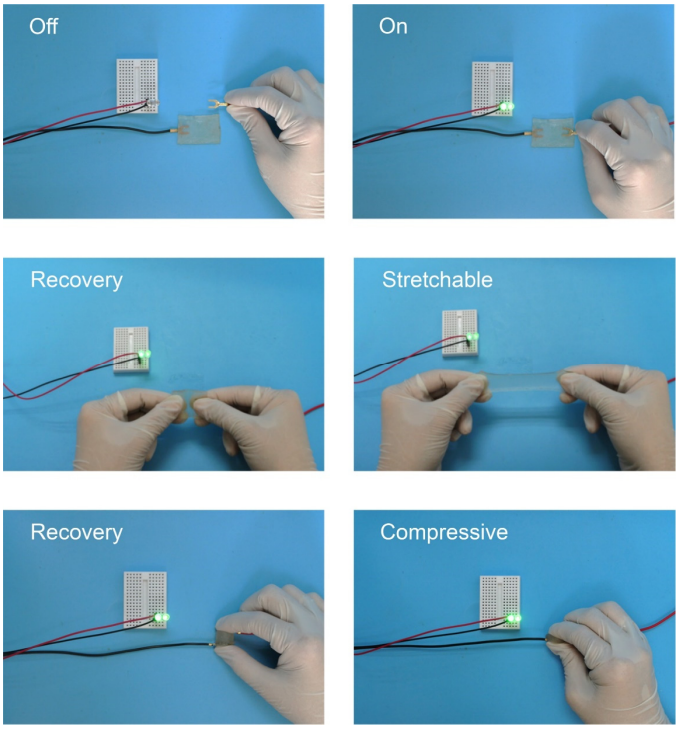

Fig. S27. Photographs of the sweat-pH-mediated CNF/PAA hydrogel to light up LEDs under different conditions.

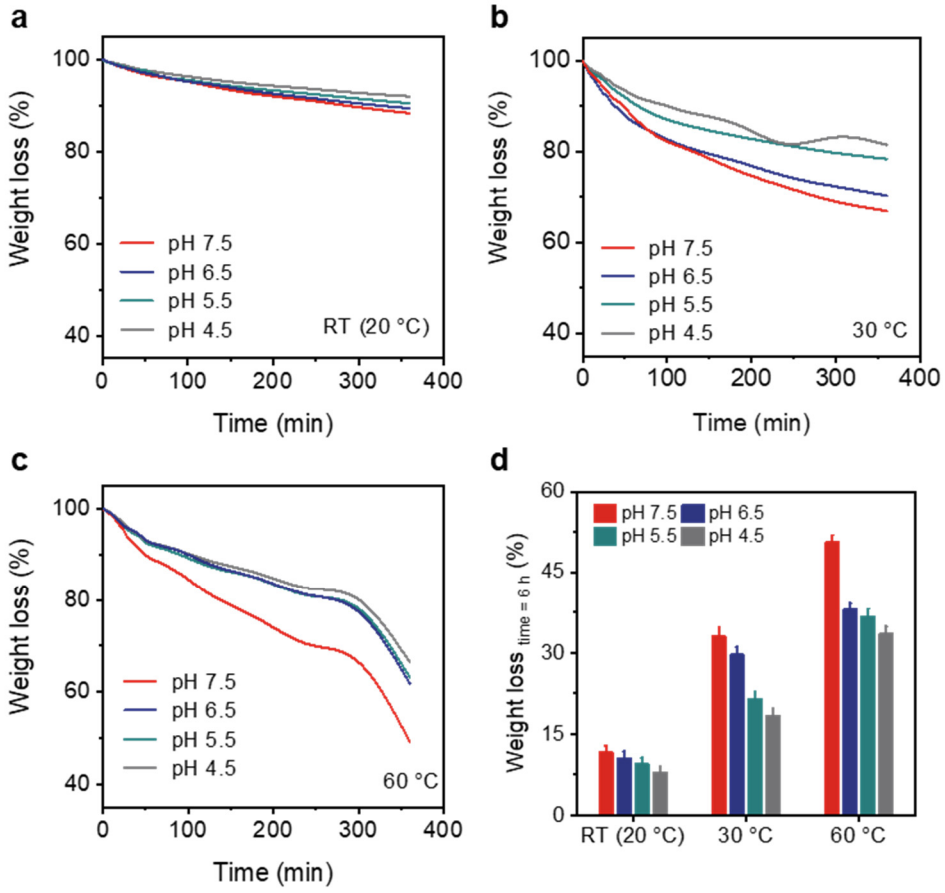

Fig. S28. Weight loss curves of hydrogels with different pH with drying time at drying temperatures of (a) RT (20 °C), (b) 30 °C and (c) 60 °C, respectively. (d) Comparisons of equilibrium weight loss of hydrogels with different pH with drying time.

The weight loss curves of CNF/PAA hydrogels with different pH at varying temperatures over time are shown in Fig. S28 a-c, and it can be observed that all hydrogels inevitably lose mass with drying time at drying temperature of RT (20 °C), 30 °C, and 60 °C. Interestingly, at the same drying temperature, hydrogels at relatively low pH (such as pH 4.5) exhibit smaller weight loss (both loss rate and volume) than those at relatively high pH (such as pH 7.5), indicating a good water retention.

Typically, we found that the weight loss of hydrogels was still within 15% after plasing at RT (20 °C) for 6 h, indicating that hydrogels are stable in air storage at RT (Fig. S28d). Unexpectedly, the weight loss of the hydrogel at pH 4.5 was still only 33.56% after existing at 60°C for 6 h, and this low value of water loss is attributed to the fact that a large number of hydrophilic polymers are tightly combined with water molecules in the network structure of the hydrogel. Hence, restricting the free movement and volatilization of water molecules.

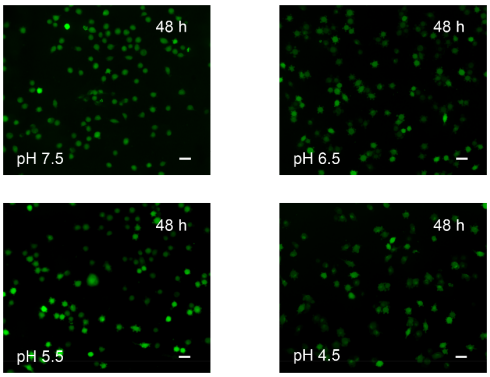

Fig. S29. Biocompatibility test of the CNF/PAA hydrogel as the pH changed. Scale bar, 50 μm. Representative fluorescent staining images of live (green) and dead (red) assay of L929 fibroblast cells, demonstrated a good cytocompatibility of the hydrogel, presented its conformal and intimate contact with human skin, which was of great significance for e-skin application.[4]

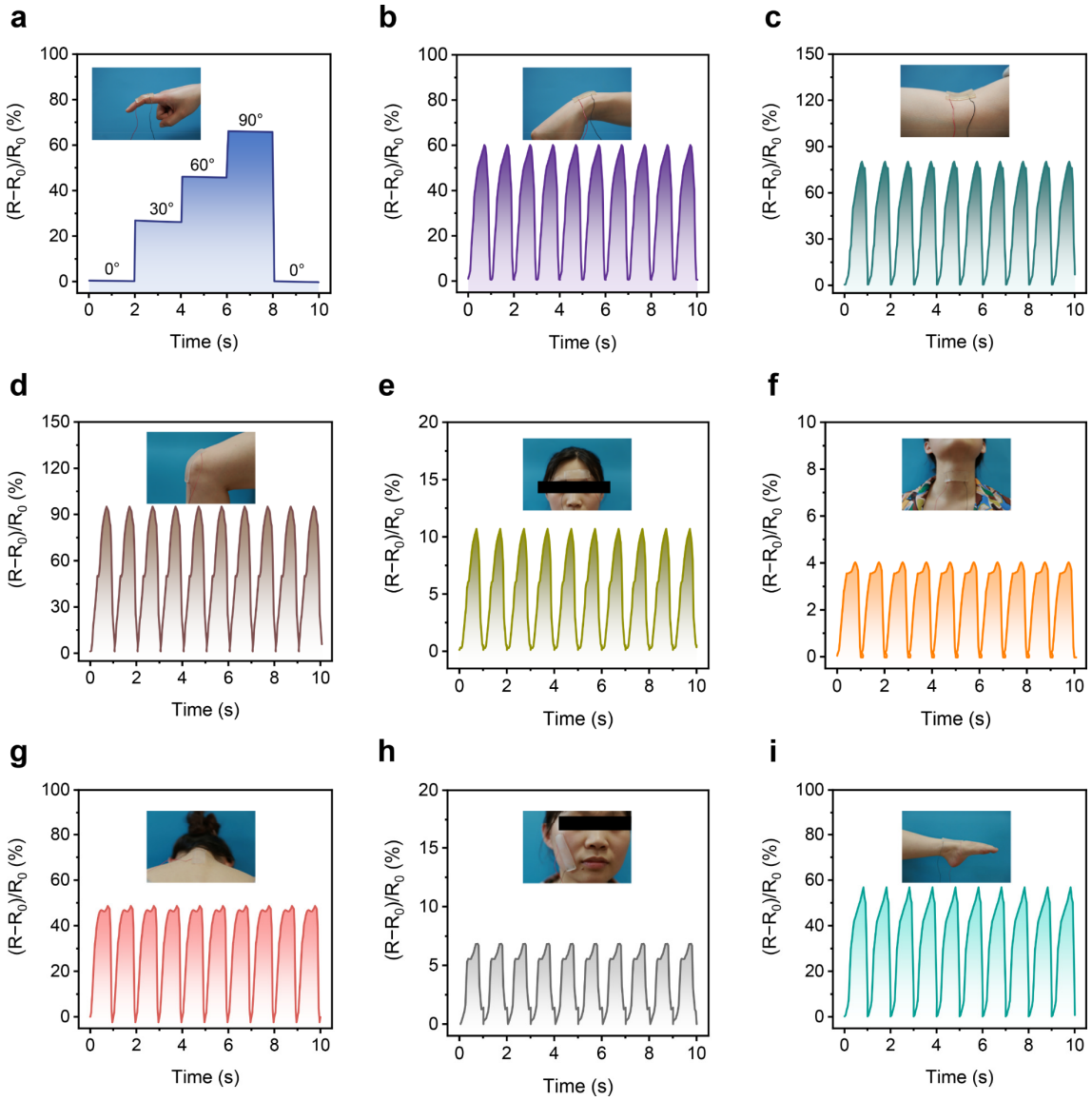

Fig. S30. Application of the CNF/PAA hydrogel as a sensor for whole-body physiological and motion monitoring. Real-time monitoring of human physical activities based on wearable sensors assembled from sweat-pH-mediated hydrogels. (a−d) Monitoring large-scale motion of human joints (the corresponding images (inset) is including finger, wrist, elbow, and knee). (e−i) Monitoring various subtle actions (the corresponding images (inset) is including frowning, swallowing, nodding, speaking, and walking).

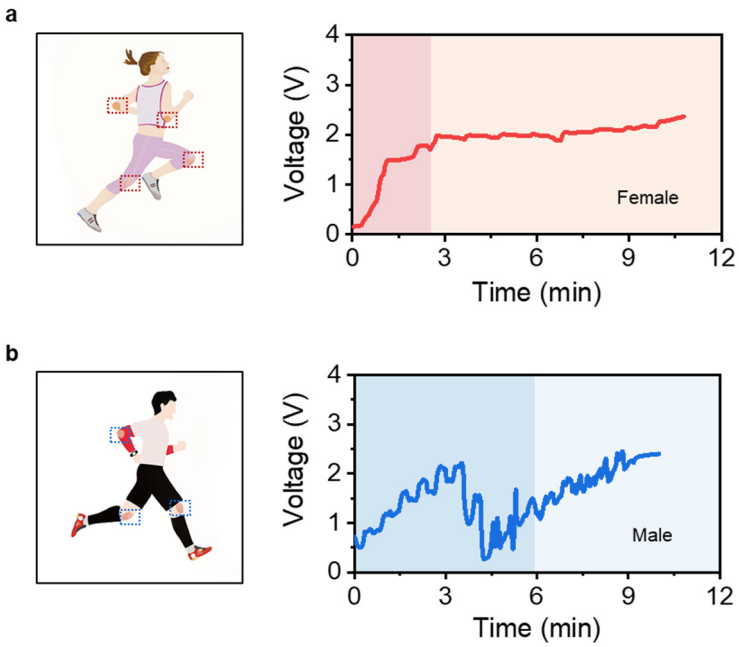

Fig. S31. The sensor assembled based on our hydrogels are used for continuous real-time monitoring of human body including (a) female and (b) male movements accompanied by changing pH during exercise.

Combining the excellent ionic conductivity and sensing properties of CNF/PAA hydrogels under varying pH, we assembled them as sensors for real-world scenarios (Figure R14). When volunteers including female (Fig. S31a) and male (Fig. S31b) exercise, it can be found that significant voltage responses are displayed consistently during workout, suggesting excellent sensing performance despite accompanying real-time changing pH. Therefore, the sensor assembled based on our hydrogels exhibits great potential for real-world applications.

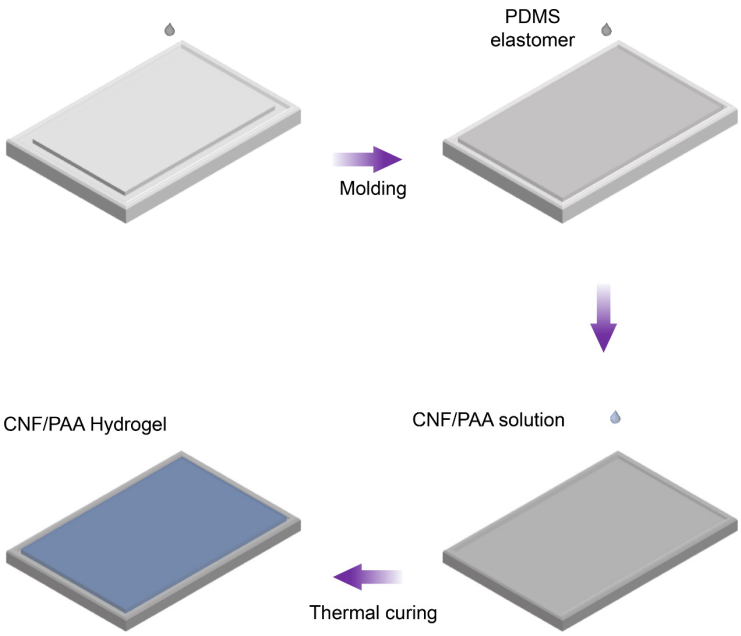

Fig. S32. Schematic illustration of fabricating the two-layer structured pH-adhesive-detachable -based triboelectric nanogenerator (pAd-TENG). The pAd-TENG was composed of a silicone rubber layer (polydimethylsiloxane, PDMS) as the tribo-negative material and the hydrogel (CNF/PAA) as both the ionic current collector and the pH-adhesive-detachable substrate.

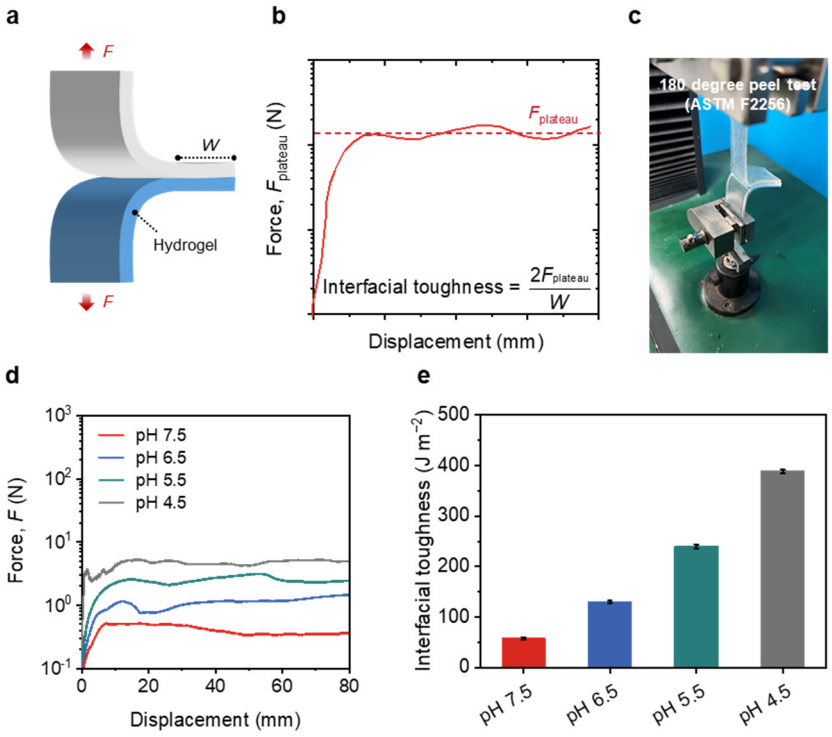

Fig. S33. (a) Schematic diagram of the 180-degree peel test of the hydrogel. (b, c) Setup and photograph for measurement of interfacial toughness based on the 180-degree peel test (ASTM F2256). (d, e) Plateau force–displacement curves and interfacial toughness for the CNF/PAA hydrogel at pH 7.5–4.5.

The schematic diagram of the peel test between the PDMS elastomer and the CNF/PAA hydrogel is shown in Fig. S33a. The peel force-displacement curve is obtained from the test, and then the interface toughness can be calculated by using the formula (Fig. S33b). The photograph of the 180-degree peel test is shown in Fig. S33c, and the PDMS and the CNF/PAA hydrogel can can be peeled stably. As displayed in Fig. S33d, as the pH decreases from 7.5 to 4.5, the $F_{plateau}$ between the elastomer and the hydrogel shows an increasing trend, implying an enhanced adhesion behaviour. Furthermore, it can be observed that the interfacial toughness is 388.6 and 57.7 J m^{-2} at pH 7.5 and 4.5, respectively, revealing a tough adhesion between the PDMS elastomer and the CNF/PAA hydrogel over a wide range of sweat pH (4.5−**7.5**), this is due to the formation of tight hydrogen bonds between the exposed −COOH and −OH on the surface of the hydrogel and −OH from PDMS (Fig. S33e).

Therefore, the PDMS elastomer and CNF/PAA hydrogels remain excellent adhesion properties in the whole pH range of sweat, which ensures desirable connection between the assembled TENGs to avoid poor contact and signal distortion in signal collection.

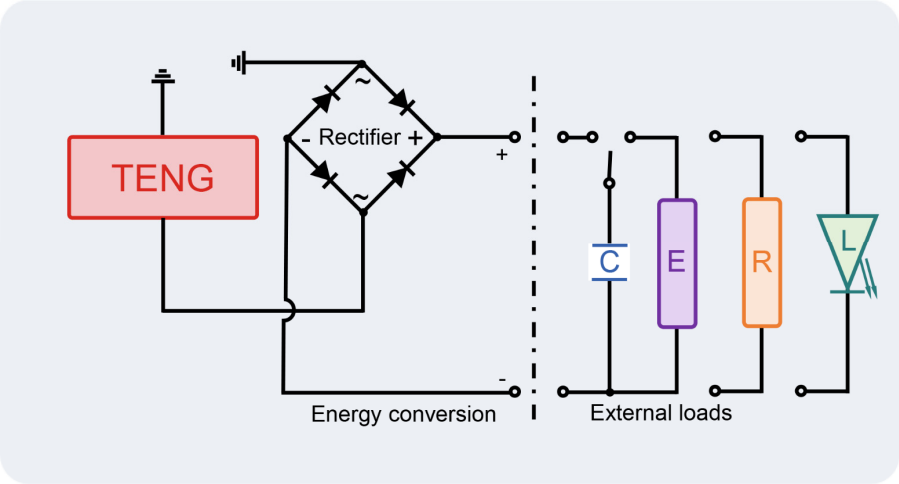

Fig. S34. Schematic diagram of the circuit with external loads.

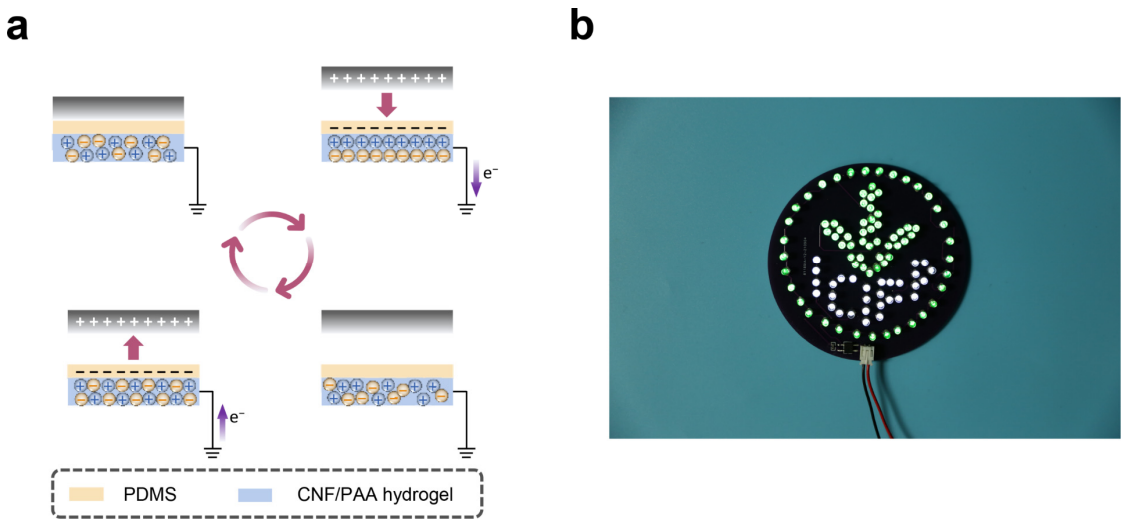

Fig. S35. Working mechanism of the pAd-TENG. (a) the working principle and corresponding signal generation of the pAd-TENG. (b) Photograph of 104 LEDs powered by hand tapping.

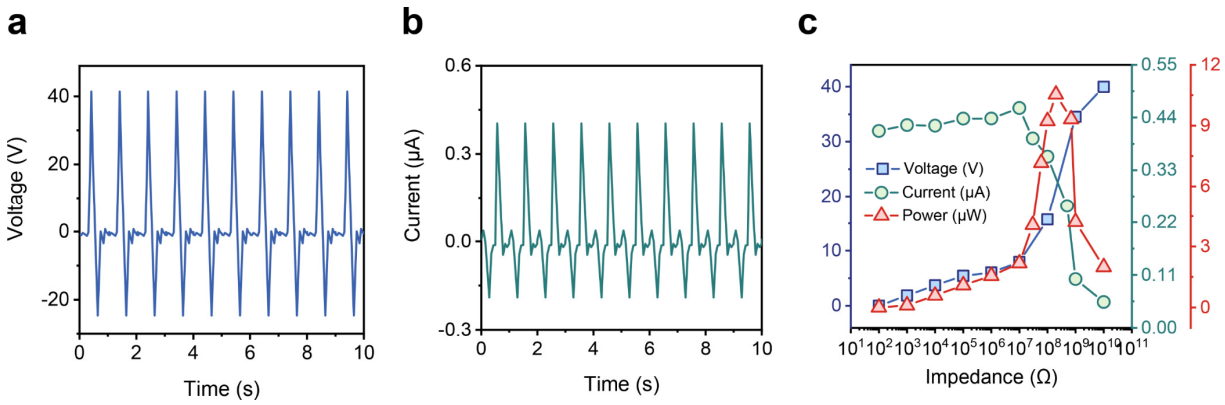

Fig. S36. Electrical performance of the pAd-TENG. (a, b) Voltage and current output waveform of the pAd-TENG. (c) the relationship between power output and load resistance.

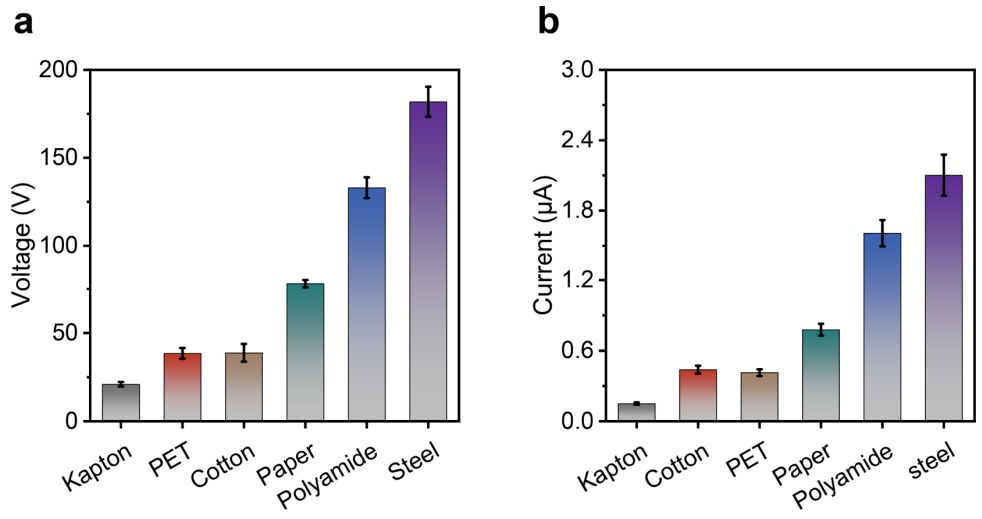

Fig. S37. Electrical behavior of the pAd-TENG. (a, b) the triboelectrification properties of various materials against pAd-TENG. As a result of the feasibility of contact electrification with any two different layers, the pAd-TENG can produce stable voltage/current outputs through the relative motion with various other materials.[5,6] The long-term motion cycles were performed to demonstrate the durability of the pAd-TENG.

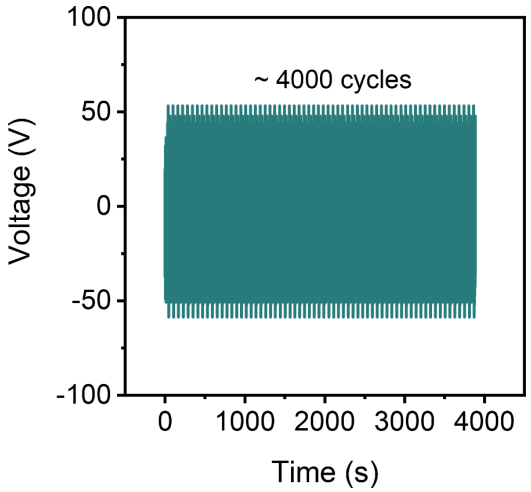

Fig. S38. Stability and durability test of the pAd-TENG.

Fig. S39. A piece of stretchable pAd-TENG-based e-skin can attach and conform to a human external wrist even under a large tilting action.

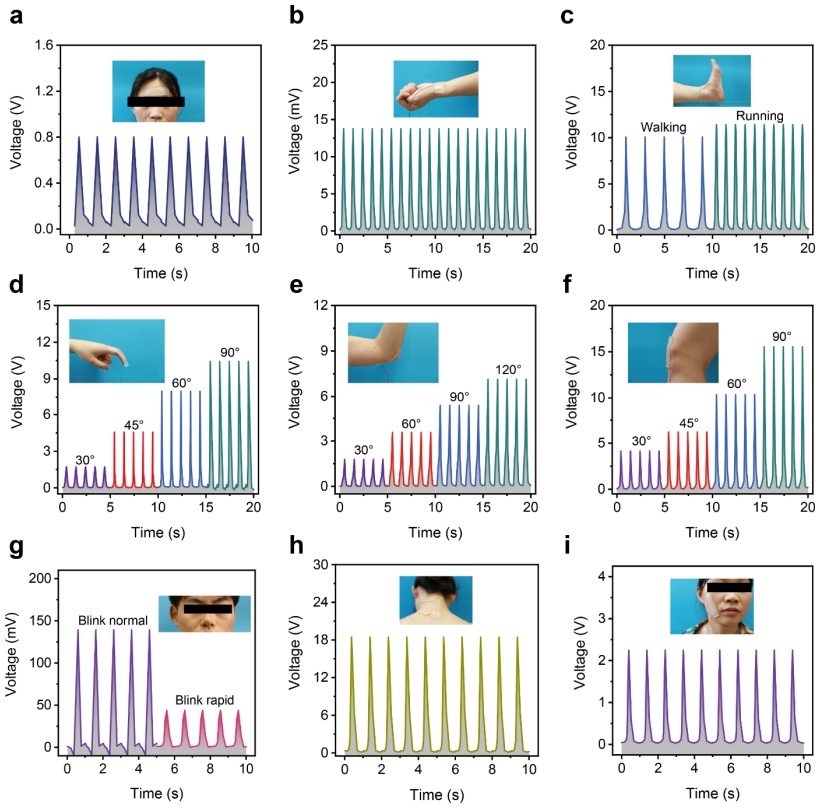

Fig. S40. Whole-body monitoring of physiological signal and joint movement. (a) Monitoring frowning behavior is performed by attaching an e-skin to the head. The photograph of the detection part of the head is inserted. (b) Real-time monitoring of the radial artery pulse by attaching an e-skin to the wrist. The photograph of the detection part of the wrist is inserted. (c) Detection of the foot motion by fixing an e-skin on the heel. The photograph of the detection portion of the heel is inserted. (d) Monitoring of the bending angles of the fingers by attaching an e-skin to the knuckle. The photograph of the detection portion of the knuckle is inserted. (e) Monitoring of the arm flexion by attaching an e-skin to the elbow. The photograph of the detection portion of the elbow is inserted. (f) Monitoring of the angle of the leg swing by attaching an e-skin to the knee. The photograph of the detection portion of the knee is inserted. (g) Monitoring blinking behavior is performed by attaching an e-skin to the eyelid. The photograph of the detection part of the eyelid is inserted. (h) Monitoring nodding behavior is performed by attaching an e-skin to the neck. The photograph of the detection portion of the neck is inserted. (i) Detection of the face motion by fixing an e-skin on the face. The photograph of the detection portion of the face is inserted.

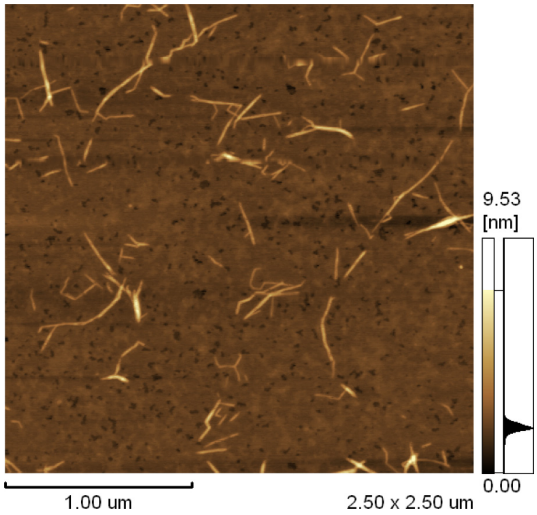

Fig. S41. AFM image of the CNFs. The width of individual nanofibril is 9.53 nm, and the length of individual nanofibril is estimated to range from200-800 nm.

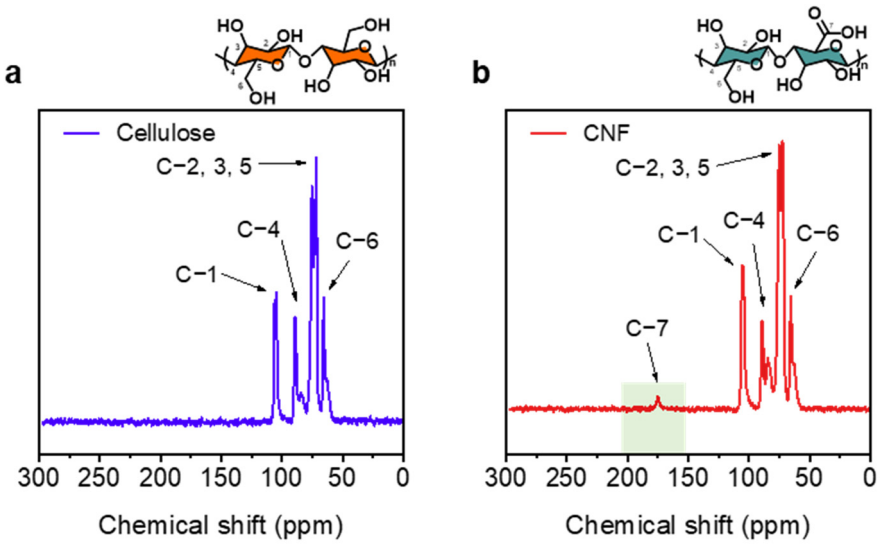

Fig. S42. Solid-state ^{13}C NMR spectra of the (a) cellulose and (b) CNF sample.

For the cellulose sample, the characteristic peaks located at 71.7 and 75.2 ppm are associated with the C-2, C-3, and C-5, peak at 89.2 ppm belongs to C-4, peak at 104.4 ppm corresponds to the C-1, and peak at 65.3 ppm is attribute to the C-6. For the CNF sample, the characteristic peaks located at 73.4 and 76.0 ppm are associated with the C-2, C-3, and C-5, peak at 89.8 ppm belongs to C-4, peak at 105.9 ppm corresponds to the C-1, and peak at 66.2 ppm is attribute to the C-6. No significant chemical shift is found in these characteristic peaks compared with the cellulose sample, indicating that its chemical environment is not changed. Apparently, a new characteristic peak is observed at 171.3 ppm belonging to the carboxyl group (−COOH) of C-7, indicating that CNF is successfully prepared.[7]

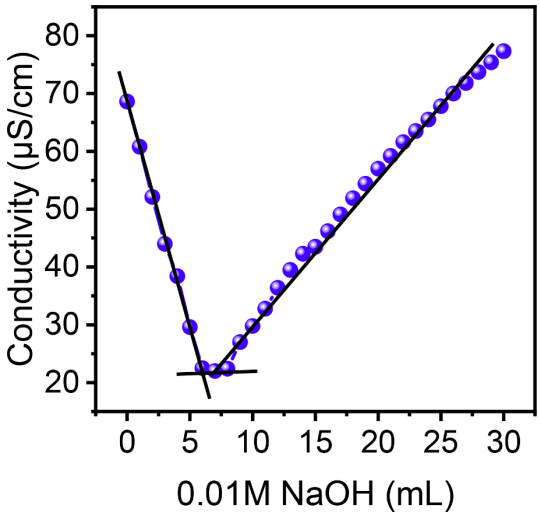

Fig. S43. Typical conductometric titration curve of the CNFs for determining the surface charge density. After TEMPO-catalyzed oxidation, C-6 hydroxyl groups of CNFs are converted to negatively charged carboxyl groups. To acquire the exact charge density, a conductive titration is calculated to be 1.75 mmol/g.[8]

Table S1. Comparison of the mechanical performance of the CNF/PAA hydrogel at pH 7.5 with other adhesive materials.

References	Adhesive materials	Tensile strength (MPa)	Compressive strength (MPa)
This work	CNF/PAA	0.083	38.39
29	BCD/PDA/XL-MSN	0.01	0.08
30	DA-Fe-PAA	0.0125	0.28
31	PEDOT:SL-PAA	0.03	0.0675
32	Fe-sL-g-PAA	0.05	0.42
33	Fe^{3+}/P(AA-co-Ls)	0.06	0.18
35	NPs-P-PAA	0.12	0.05
34	LS_x	0.077	0.28
37	PSG-PEDOT-PAM	0.06	16

Table S2. Comparison of the interfacial toughness of the CNF/PAA hydrogel at pH 4.5 with other adhesive materials on the different engineering materials.

References	Adhesive materials	Interfacial toughness on the different engineering materials (J/m^2)
This work	CNF/PAA	453
28	Hybrid ionic skin	400
42	SACP	160
38	Nucleobase-tackified	300
8	PAA/betaine	180
39	MASLD	94
43	STSMH	30
41	PTCM-Gly	125
40	PAAm@κ-carrageenan hydrogel	250
44	BAP	60

Table S3. Comparison of the interfacial toughness of the CNF/PAA hydrogel at pH 4.5 with other adhesive materials on the skin.

References	Adhesive materials	Interfacial toughness on the surface of the skin (J/m^2)
This work	CNF/PAA	453
35	NPs-P-PAA	32.5
45	PAM/PDA/XL-MSN	160
44	BAP	50
8	PAA/betaine	180
47	PGAQ-GelMA	12
46	PAAc-ChCl-EG	100
43	STSMH	40
28	Hybrid ionic skin	200
48	Bioadhesive	350

Supplementary References

1 S. Wang, L. Yu, S. Wang, L. Zhang, L. Chen, X. Xu, Z. Song, H. Liu, C. Chen, *Nat*. *Commun*., 2022, **13**, 3408.

2 Y. Ye, H. Oguzlu, J. Zhu, P. Zhu, P. Yang, Y. Zhu, Z. Wang, O. J. Rojas, F. Jiang, *Adv*. *Funct*. *Mater*., 2022, 2209787.

3 A. Isogai, T. Saito, H. Fukuzumi. *Nanoscale*, 2011, **3**, 71.

4 M. Gao, H. Wu, R. Plamthottam, Z. Xie, Y. Liu, J. Hu, S. Wu, L. Wu, X. He, Q. Pei, Skin temperature-triggered, debonding-on-demand sticker for a self-powered mechanosensitive communication system. *Matter*, 2021, **4**, 1962-1974.

5 H. Zou, Y. Zhang, L. Guo, P. Wang, X. He, G. Dai, H. Zheng, C. Chen, A. C. Wang, C. Xu, Z. L. Wang, Quantifying the triboelectric series. *Nat*. *Commun*., 2019, **10**, 1427.

6 Y. Wu, J. Qu, X. Zhang, K. AO, Z. Zhou, Z. Zheng,Y. Mu, X. Wu, Y. Luo, S. P. Feng, Biomechanical energy harvesters based on ionic conductive organohydrogels via the hofmeister effect and electrostatic interaction. *ACS Nano*, 2021, **15**, 13427-13435.

7 L. Wang, H. Zhu, G. Xu, X. Hou, H. He, S. Wang, A biocompatible cellulose-nanofiber-based multifunctional material for Fe^{3+} detection and drug delivery. *J*. *Mater*. *Chem*. *C*, 2020, **8**, 11796-11804.

8 A. Isogai, T. Saito, H. Fukuzumi, TEMPO-oxidized cellulose nanofibers. *Nanoscale*, 2011, **3**, 71-85.